Elastic vibrations of a fiber due to impact of an aerosol particle and their influence on the efficiency of fibrous filters

A. L. Chernyakov,[1] A. A. Kirsch,[1] and V. A. Kirsch[2]
[1]*National Research Center "Kurchatov Institute," Kurchatov Square 1, 123182 Moscow, Russia*
[2]*A. N. Frumkin Institute of Physical Chemistry and Electrochemistry, Russian Academy of Sciences, Leninsky Prospekt 31, 119991 Moscow, Russia*
(Received 20 April 2010; revised manuscript received 15 February 2011; published 4 May 2011)

The excitation of sound vibrations of a cylindrical fine fiber due to the impact of a spherical aerosol particle is investigated. The equations describing the dynamics of impact are derived for an arbitrary shooting parameter. The coefficient of restitution is calculated, and its analytical approximation is obtained. It is shown, for the case of long fibers, that the coefficient of restitution depends upon a single parameter λ_c. The parameter λ_c depends on the particle radial velocity component near the fiber surface, the mass of the particle, the density of the fiber, the modulus of elasticity, and the geometric parameters of the fiber and the particle. The inertial deposition of submicron aerosol particles on fine fibers in a filter is considered. The efficiency of filtration is studied as a function of the gas flow velocity. The existence of a critical flow velocity U^*, below which the losses of particle energy during collision have no effect on the efficiency, is demonstrated. For velocities higher than the critical velocity, the filtration efficiency is dependent on the mechanisms of nonelastic losses of the particle's energy. Its value can be significantly lower than that estimated when particle rebound effects are neglected. After they have rebounded, some particles are not able to attain the initial high velocities in the stream, thus depositing on neighboring fibers. The dynamics of these particles is investigated. For this case, it is shown that the filtration efficiency is dependent on the velocity distribution of the rebounded particles and that it increases with the packing density of fibers. A qualitative difference between the asymptotic behavior of a fiber and that of a flat plate is found long after the initial impulse.

DOI: 10.1103/PhysRevE.83.056303 PACS number(s): 47.55.D−, 82.70.Rr, 47.56.+r, 47.15.G−

I. INTRODUCTION

A high-efficiency air cleaning from fine suspended particles is of key importance for several advanced technologies and for environmental protection. Air cleaning is performed by filtering materials consisting of a large number of layers of fine fibers. Among various filtering materials, the fibrous filters have a minimal resistance to air flow at a given filter collection efficiency. The deposition of suspended particles upon fibers within the filter occurs due to their diffusional or inertial shift from the streamlines toward the fiber surface. The surface forces attract and hold the particles that are touching the fiber surface. To provide minimal pressure drop, filters are used with low flow velocities of the order a few centimeters per second. In this case for particles with a density of 1–2 g/cm^3, the inertial deposition may be neglected. However, in the case of filtration of the fine particles of heavy metals, both the inertia of particles and the mechanisms of the particle-fiber interaction must be accounted for. This problem is of great importance to many industries, including the atomic energy industry.

A characteristic of heavy particle collection is the influence of gravity on the filtration efficiency at small flow velocities [1] and particle rebound from fibers at high flow velocities, as, for example, in the case of air sampling with analytical filters. A decrease in the collection efficiency with an increase in the face velocity has been observed experimentally [2–6]. However, to date, no theoretical estimations of inertial deposition of aerosol particles on fine fibers that account for their contact interaction during collision have been performed.

When considering the collection of submicron aerosol particles with high density in the inertial regime with possible rebound from fibers, the effect of gravity on the efficiency of capture can be neglected together with that due to diffusion. Relative particle velocity in the gas stream is not high; thus, the drag force acting on the particle is given by Stokes's law. The inertial deposition of particles on fibers from the stream is governed by the dimensionless Stokes number,

$$\mathrm{St} = \frac{C_1 m U_0}{6\pi\mu R r_0},$$

where C_1 is the Cunningham correction factor accounting for the gas slip on the particle surface [1], m is the mass of the particle, R is the particle radius, U_0 is the undisturbed (face) flow velocity before the filter, μ is the dynamic viscosity of the gas, and r_0 is the fiber radius.

When the Stokes number is small, $\mathrm{St} \ll 1$, the filter efficiency is determined by the mechanism responsible for the capture of the aerosol particle by the fiber surface. Generally, basic mechanisms of capture are the convective diffusion in the gas flow or the movement due to external force fields [1]. The contact interaction of a particle with a fiber by itself has a small effect on the collection efficiency.

For high velocities and heavy particles, the Stokes number may well exceed unity. In this case, if no rebound is considered, the fiber collection efficiency tends to the constant value (ballistic limit), which is the case for large droplets [7,8]. The rebound is important for solid particles at $\mathrm{St} \geqslant 1$. In this case, the efficiency of deposition of particles is governed by the mechanisms of particle energy losses during contact,

like any dissipative process or loss of energy due to emission of long-wave transverse waves [6]. For some conditions, the particle energy losses are solely connected with the excitation of transverse sound waves propagating along a fiber.

Timoshenko, in 1912, was the first to consider the excitation of transverse vibrations of a beam at impact [9,10]. Energy losses due to sound emission during the ball-plate collision were considered in subsequent studies [6,11,12]. In general, the investigation of particle rebound from solid surfaces has gained significant attention. An entire issue of *Aerosol Science and Technology* [13] was devoted to reviews on the subject. References to later works can be found in Refs. [14,15]. However, to our knowledge, there are no theoretical works investigating the losses of energy due to the sound emission when a heavy macroparticle collides with a fine fiber. In the present work, we consider the collision of a heavy aerosol particle with a fine cylindrical fiber at an arbitrary shooting distance and with van der Waals forces.

The remainder of this paper is organized as follows. Section II deals with the excitation of sound vibrations in fine fibers during impact with an aerosol particle at an arbitrary shooting parameter and with van der Waals and friction forces. For high-velocity particles having a kinetic energy greater than adhesion energy, an equation for the coefficient of restitution is derived, which differs from the equation describing the particle-plate collision. The derived equation is solved numerically, and the corresponding analytic approximation for the restitution coefficient is found.

Using this approximation, in Sec. III we estimate the critical initial velocities of particles defined so that the particles that have greater velocities rebound from fibers at high Stokes numbers. The values of the critical velocities are compared with those computed from the solution of the complete system of equations derived in Sec. II. Conditions are found under which the losses of the particle energy due to different nonelastic processes are negligibly small.

In Sec. IV, the formula for the coefficient of restitution, derived in Sec. II, is applied for calculating the single-fiber collection efficiency for aerosol particles in a model fibrous filter. A plane gas flow field for a system of parallel fibers is used. The particle trajectories are calculated at moderate velocities with St ~ 1. A decrease in the collection efficiency due to rebound of particles is found. A qualitative comparison of the obtained results with the experiment is done.

In Sec. V, a simple model of aerosol filtration with a fibrous filter is considered for the case of high Stokes numbers and for conditions when the particles have no time to attain the flow velocity between sequential collisions with fibers. The dependence of the coefficient of the particle penetration versus the filter packing density is found using the Monte Carlo technique.

In Appendix A, the dynamics of elastic deformation of a fiber and a plate after initial impulse are compared. A significant difference between the fiber and the plate deformations is found at large times. In Appendix B, a simplified model for the multiple collisions of a particle with fibers is given. The method of calculation of the retarded and instantaneous van der Waals forces is given in Appendix C.

II. EXCITATION OF LONG-WAVE ELASTIC VIBRATIONS IN A FIBER AT THE IMPACT OF AN AEROSOL PARTICLE

Consider the collision of a spherical aerosol particle of radius R with a fiber having radius r_0 and length L and aligned along the z axis, as shown in Fig. 1. Suppose that the vector of the initial velocity of the particle lies in a plane perpendicular to the axis of the fiber at $z = z_0$.

The equation of the transverse displacement of the fiber due to the action of the point force $\mathbf{F}$ is

$$\rho S \frac{\partial^2 \boldsymbol{\xi}}{\partial t^2} = -EI \frac{\partial^4 \boldsymbol{\xi}}{\partial z^4} - \delta(z - z_0)\mathbf{F}(t). \tag{1}$$

Here $\boldsymbol{\xi} \equiv \boldsymbol{\xi}(z,t)$ is the transverse displacement of the fiber from its initial position, $\delta(z)$ is Dirac's delta function, ρ is the fiber density, S is the surface of the cross section, E is Young's modulus, and I is the moment of inertia of the fiber cross section [16]. The equation describing the fiber vibrations (1) should be supplemented with boundary conditions. Assume that the fiber is fixed at the ends

$$\boldsymbol{\xi}(0,t) = \boldsymbol{\xi}(L,t) = 0.$$

The equation of vibrations of a fiber with fixed ends (1) should be coupled with the equation of motion of the vector $\mathbf{r}$, defining the position of a particle with mass m:

$$m \frac{d^2\mathbf{r}}{dt^2} = \mathbf{F}(t) = \mathbf{F}_w(t) + \mathbf{F}_e(t). \tag{2}$$

The force $\mathbf{F}$ is governed by its long-range part $\mathbf{F}_w$ acting in the gap when $s \equiv |\mathbf{r}(t) - \boldsymbol{\xi}(z_0,t)| - (R + r_0) > 0$ and is governed by the force of elastic interaction of a spherical particle and a fiber $\mathbf{F}_e$ at $s < 0$. We consider the interaction of a particle with a fiber under the action of the nonretarded van der Waals forces. The van der Waals (dispersion) forces significantly contribute to the particle-fiber interaction dynamics at small distances $s < \min(R,r_0)$, where one can use the following formula for the van der Waals force [17]:

$$\mathbf{F}_w = -\frac{\mathbf{r}(t) - \boldsymbol{\xi}(z_0,t)}{|\mathbf{r}(t) - \boldsymbol{\xi}(z_0,t)|}\left[\frac{1}{(s+\varepsilon)^2} - \frac{\varepsilon}{(10s+\varepsilon)^3}\right] \times \frac{AR}{6}\left(\frac{r_0}{R+r_0}\right)^{1/2}\theta(s), \tag{3}$$

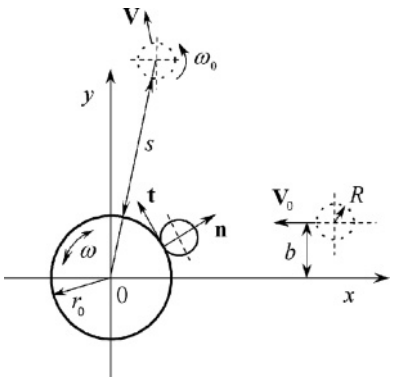

FIG. 1. Sketch of the particle-fiber interaction during collision at high Stokes numbers.

where $\varepsilon = 4 \times 10^{-8}$ cm is the adhesion distance, A is Hamaker's constant, and $\theta(s)$ is the Heaviside step function, which is 1 if s is greater than 0 and 0 if s is less than 0. The second term in parentheses in Eq. (3) was added to provide a continuity of the interaction force $\mathbf{F} = \mathbf{F}_w + \mathbf{F}_e$ at $s = 0$ for numerical stability of the computations. The force of elastic interaction is found from the theory of Hertz [16,18]:

$$\mathbf{F}_e = \frac{\mathbf{r}(t) - \boldsymbol{\xi}(z_0,t)}{|\mathbf{r}(t) - \boldsymbol{\xi}(z_0,t)|} K(-s)^{3/2}\theta(-s). \tag{4}$$

The coefficient K depends on Young's modulus of the fiber E and that of the particle E', their Poisson coefficients σ and σ', and the fiber and particle shapes and dimensions. For a spherical particle of radius R and a cylindrical fiber with radius r_0 we have [16]

$$\begin{aligned} K &= \frac{1}{D}\frac{R^{1/2}}{(1 + R/r_0)^{1/4}} f(e), \\ D &= \frac{3}{4}\left(\frac{1-\sigma^2}{E} + \frac{1-\sigma'^2}{E'}\right) \equiv \frac{3}{4E^*}. \end{aligned} \tag{5}$$

The eccentricity of the elliptic region of contact e is found from the relation

$$\frac{(1-e^2)^{-1}E(e) - K(e)}{K(e) - E(e)} = 1 + \frac{R}{r_0}, \tag{6}$$

where $K(e)$ and $E(e)$ are complete elliptic integrals of the first and second kind, respectively. The function $f(e)$ is

$$f(e) = \frac{\pi}{2^{1/2}} \frac{[K(e) - E(e)][(1-e^2)^{-1}E(e) - K(e)]}{eK(e)^{3/2}}. \tag{7}$$

The larger semiaxis a of the elliptical region of contact and the surface of the contact region S_c are

$$a = (F_e D R)^{1/3}\left(1 + \frac{R}{r_0}\right)^{-1/6} f_1(e),$$

$$S_c = \pi a^2(1-e^2)^{1/2} = \pi(F_e D R)^{2/3}\left(1 + \frac{R}{r_0}\right)^{-1/3} f_2(e),$$

where

$$f_1(e) = \left(\frac{4}{\pi e^2}\right)^{1/3} \{[K(e) - E(e)][(1-e^2)^{-1}E(e) - K(e)]\}^{1/6},$$

$$f_2(e) = (1-e^2)^{1/2} f_1(e)^2.$$

The maximal stress in the center of contact is given by

$$\sigma_{\max} = \frac{3F_e}{2S_c} = \frac{3}{2\pi}\frac{F_e^{1/3}}{(DR)^{2/3}}\left(1 + \frac{R}{r_0}\right)^{1/3} f_2^{-1}(e).$$

The dependencies of the eccentricity $e(R/r_0)$ and the functions $f[e(R/r_0)]$, $f_1[e(R/r_0)]$, $f_2[e(R/r_0)]$ on the ratio of the particle to fiber radii are shown in Fig. 2. It is seen that the functions $f(R/r_0)$ and $f_2(R/r_0)$ are almost unchanged and are near a value of 1 over a significant interval. The dependence of the force on the gap for $s \sim \varepsilon$ is illustrated in Fig. 3 for three values of the radius of the particle interacting with the fiber.

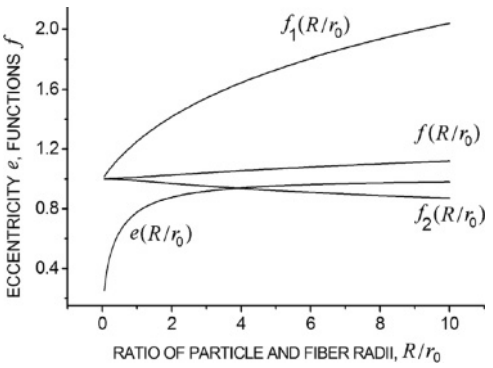

FIG. 2. The eccentricity of the elliptic region of contact e and the functions f, f_1, f_2, defining the parameter K in the formula of Hertz, the bigger semiaxis of ellipse a, and its surface S_c, respectively, vs the ratio of the particle to fiber radii.

At the initial moment the fiber is at rest,

$$\boldsymbol{\xi}(z,0) = 0, \quad \dot{\boldsymbol{\xi}}(z,0) = 0,$$

while the particle is moving with the velocity $\mathbf{V}_0$,

$$\dot{\mathbf{r}}(0) = \mathbf{V}_0,$$

and with the shooting parameter b. The displacement of the fiber at the point of contact may be expressed in terms of eigenmodes of vibration,

$$\boldsymbol{\xi}(z,t) = \sum_n \boldsymbol{\xi}_n(t) \sin\left(\frac{\pi n}{L} z\right).$$

Inserting this expression into Eq. (1), we obtain equations for the amplitudes $\xi_n(t)$:

$$\frac{d^2\boldsymbol{\xi}_n}{dt^2} = -\omega_n^2 \boldsymbol{\xi}_n - \frac{2}{\rho S L}\sin\left(\frac{\pi n}{L} z_0\right) \mathbf{F}[\mathbf{r} - \boldsymbol{\xi}(z_0,t)], \tag{8}$$

where n is the mode number, $\omega_n = \beta_c \pi^2 n^2 / L^2$ is the eigenfrequency, $\beta_c = (EI/\rho S)^{1/2}$, and z_0 is the coordinate of

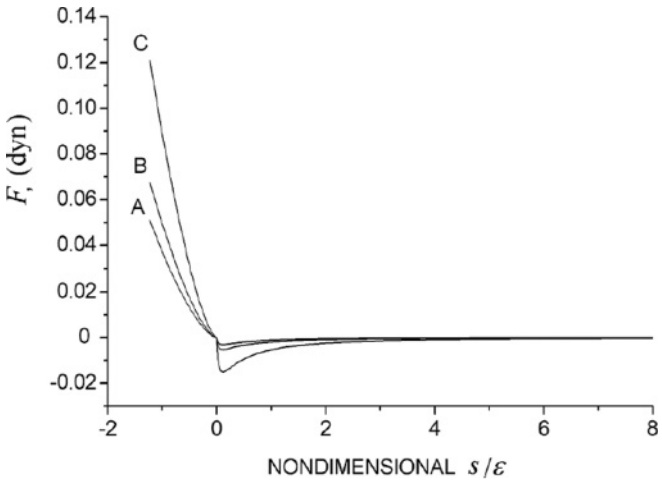

FIG. 3. The force of interaction between a spherical particle with radius $R = 0.5$ (curve A), 1 (curve B), and 3 μm (curve C) and a cylindrical fiber with radius $r_0 = 1$ μm vs distance between their nondeformed surfaces: $A = 10^{-12}$ erg, $\varepsilon = 4 \times 10^{-4}$ μm, $\sigma = \sigma' = 0.3$, and $E = E' = 10^{12}$ erg/cm^3.

the point of impact. Assume that the vibrations are damping with the decrement $\nu_n \ll \omega_n$. Then, Eq. (8) is reduced to the following form:

$$\frac{d^2\boldsymbol{\xi}_n}{dt^2} = -\omega_n^2\boldsymbol{\xi}_n - 2\nu_n\frac{d\boldsymbol{\xi}_n}{dt} - \frac{2}{\rho SL}\sin\left(\frac{\pi n}{L}z_0\right)\mathbf{F}[\mathbf{r}-\boldsymbol{\xi}(z_0,t)]. \tag{9}$$

The velocity and the displacement of the point of interaction can be expressed in terms of force integrals:

$$\frac{d}{dt}\boldsymbol{\xi}(z_0,t) = -\int_0^t \frac{2}{\rho SL}\left\{\sum_n \sin^2\left(\frac{\pi n}{L}z_0\right)\exp[-\nu_n(t-t')] \times \cos[\omega_n(t-t')]\right\}\mathbf{F}(t')dt', \tag{10}$$

$$\boldsymbol{\xi}(z_0,t) = -\int_0^t \frac{2}{\rho SL}\left\{\sum_n \sin^2\left(\frac{\pi n}{L}z_0\right)\exp[-\nu_n(t-t')] \times \frac{\sin[\omega_n(t-t')]}{\omega_n}\right\}\mathbf{F}(t')dt'. \tag{11}$$

If the particle collides with the center of the fiber, then the odd-n modes remain. For the nonzero shooting parameter b and accounting for the friction force, one has to consider not only the flexural but also the torsional vibrations. It is convenient to introduce unit vectors $\mathbf{e}_z$, $\mathbf{n}$, and $\mathbf{t}$:

$$\mathbf{n}(t) = \frac{\mathbf{r}(t)-\boldsymbol{\xi}(z_0,t)}{|\mathbf{r}(t)-\boldsymbol{\xi}(z_0,t)|}, \mathbf{t}(t) = [\mathbf{e}_z \times \mathbf{n}(t)]. \tag{12}$$

These vectors are mutually normal and are oriented along the fiber axis, along the line connecting the centers of the spherical particle and the fiber, and along the surface tangent line on the point of collision, respectively (Fig. 1). It is convenient to decompose the interaction force in terms of these vectors:

$$\mathbf{F} = \mathbf{n}F_n + \mathbf{t}F_t. \tag{13}$$

The rotation of the particle and the fiber torsional vibrations are governed by following equations:

$$I_0\frac{d\omega_0}{dt} = F_t R, \tag{14}$$

$$\rho I_1\frac{\partial^2\varphi}{\partial t^2} = C\frac{\partial^2\varphi}{\partial z^2} + r_0F_t(t)\delta(z-z_0), \tag{15}$$

where ω_0 is the angular velocity of the particle, φ is the angle of rotation of the fiber, $I_0 = 2mR^2/5$ is the particle moment of inertia, $I_1 = \pi r_0^4/2$ is the fiber moment of inertia, and $C = \pi r_0^4 E/4(1+\sigma)$ is the torsional rigidity. The velocity of propagation of the torsional waves $\tilde{\beta}_c$ is

$$\tilde{\beta}_c = \left(\frac{C}{\rho I_1}\right)^{1/2} = \left[\frac{E}{2(1+\sigma)\rho}\right]^{1/2}. \tag{16}$$

Expanding $\varphi(z,t)$ in eigenmodes, we obtain the expression for the angular velocity of the fiber ω accounting for the possible damping of the torsional vibrations:

$$\omega(z_0,t) = \int_0^t \frac{4}{\rho LSr_0}\sum_n \sin^2\left(\frac{\pi n z_0}{L}\right)\exp[-\tilde{\nu}_n(t-t')] \times \cos[\tilde{\omega}_n(t-t')]F_t(t')dt'. \tag{17}$$

The frequencies of the torsional vibrations are given by

$$\tilde{\omega}_n = \frac{\tilde{\beta}_c\pi n}{L}.$$

The force of friction is directed opposite to the tangential component of the relative velocity, and it is proportional to the normal component of the force of pressure during the collision of a particle with a fiber:

$$\mathbf{V}_t = \mathbf{t}[(\dot{\mathbf{r}}-\dot{\boldsymbol{\xi}})\cdot\mathbf{t} - \omega_0 R - \omega r_0], \tag{18}$$

$$\mathbf{F}_t = -k_t\frac{\mathbf{V}_t}{|\mathbf{V}_t|}F_n, \tag{19}$$

where k_t is the friction coefficient. The influence of the tangential force on the value of the normal force is negligible for $k_t \ll 1$ [18].

For relatively long fibers, the bending waves have no time to reach the limit $\omega_1 T \ll 1$ during the collision. Thus, without damping, Eqs. (10) and (11) are reduced to

$$\boldsymbol{\xi}(z_0,t) = -\int_0^t \frac{\mathbf{F}(t')}{\rho S\omega(k)}\sin[\omega(k)(t-t')]\frac{dk}{2\pi}dt', \tag{20}$$

$$\frac{\partial\boldsymbol{\xi}(z_0,t)}{\partial t} = -\int_0^t \frac{\mathbf{F}(t')}{\rho S}\cos[\omega(k)(t-t')]\frac{dk}{2\pi}dt'. \tag{21}$$

The frequency of vibrations of the fiber with wave number k is

$$\omega(k) = \beta_c k^2,\ \beta_c = \left(\frac{EI}{\rho S}\right)^{1/2}. \tag{22}$$

The integral over wave numbers in Eq. (21) is easily calculated:

$$\int_{-\infty}^{\infty}\cos[\beta_c k^2(t-t')]\frac{dk}{2\pi} = \left[\frac{1}{8\pi\beta_c(t-t')}\right]^{1/2}.$$

Thus, the fiber velocity at the point of interaction is given by

$$\frac{\partial\boldsymbol{\xi}(z_0,t)}{\partial t} = -\int_0^t \frac{\mathbf{F}(t')}{\rho S}\frac{1}{[8\pi\beta_c(t-t')]^{1/2}}dt'. \tag{23}$$

Similar transformations for torsional waves at $\tilde{\omega}_1 T \ll 1$ reduce Eq. (14) to the local form:

$$\omega(z_0,t) = \frac{2F_t(t)}{\rho Sr_0}. \tag{24}$$

Introducing nondimensional variables $\mathbf{r} = V_0 T\mathbf{r}'$, $\boldsymbol{\xi} = V_0 T\boldsymbol{\xi}'$, $t = T\tau$, $z = Lz'$, $r_0\omega = V_0\omega'$, and $R\omega_0 = V_0\omega_0'$ and setting $T = (m^2/K^2V_0)^{1/5}$, we arrive at a system of dimensionless equations describing the dynamics of the particle collision with a fiber:

$$\frac{d^2\mathbf{r}'}{d\tau^2} = \mathbf{F}'(\tau), \tag{25}$$

$$\frac{d}{d\tau}\boldsymbol{\xi}'(z_0',\tau) = -\int_0^\tau \frac{2m}{\rho SL}\sum_n \sin^2(\pi n z_0') \times \cos[\omega_n T(\tau-\tau')]\mathbf{F}'(\tau')d\tau', \tag{26}$$

$$\frac{d\omega_0'}{d\tau} = \frac{5}{2}F_t'(\tau), \tag{27}$$

$$\omega'(z_0',\tau) = \int_0^\tau \frac{4m}{\rho LS}\sum_n \sin^2(\pi n z_0') \times \cos[\tilde{\omega}_n T(\tau-\tau')]F_t'(\tau')d\tau', \quad (28)$$

$$F_n' = (-s')^{3/2}\theta(-s') - \lambda_2 \times \left[\frac{1}{(s'+\varepsilon')^2} - \frac{\varepsilon'}{(10s'+\varepsilon')^3}\right]\theta(s'), \quad (29)$$

where $s' \equiv |\mathbf{r}' - \boldsymbol{\xi}'(z_0'0)| - (R+r_0)/V_0T$, $\varepsilon' = \varepsilon/V_0T$, and $\theta(s')$ is the Heaviside step function. The solution of the system of Eqs. (25)–(29) is a function of the following nondimensional parameters:

$$\lambda_1 = \frac{m}{\rho SL},\ \lambda_2 = \frac{AR}{6mV_0^3T}\left(\frac{r_0}{R+r_0}\right)^{1/2},$$
$$\omega_1 T = \frac{\beta_c \pi^2 T}{L^2},\ \tilde{\omega}_1 T = \frac{\tilde{\beta}_c \pi T}{L}.$$

For long fibers, the system of equations describing the excitation of transverse waves at the zero shooting distance and in the absence of friction may be reduced to the following system:

$$\frac{d\mathbf{r}'}{d\tau} = \mathbf{V}'_n + \int_0^\tau \mathbf{F}'(\tau')d\tau', \quad (30)$$

$$\frac{\partial \boldsymbol{\xi}'(z_0,\tau)}{\partial \tau} = -\int_0^\tau \frac{\lambda_c \mathbf{F}'(\tau')}{(\tau-\tau')^{1/2}}d\tau', \quad (31)$$

where the parameter λ_c is expressed in terms of λ_1 and $\omega_1 T$,

$$\lambda_c = \frac{m}{\rho S(8\pi\beta_c T)^{1/2}} = \frac{\pi^{1/2}}{8^{1/2}}\frac{\lambda_1}{(\omega_1 T)^{1/2}}. \quad (32)$$

For the case of a spherical particle with density $\tilde{\rho}$ and a cylindrical fiber, the parameter λ_c is given by

$$\lambda_c = \frac{2}{3\pi^{7/10}}\left(\frac{R}{r_0}\right)^{5/2}\left(\frac{\tilde{\rho}}{\rho}\right)^{4/5}\left(\frac{E^*}{E}\right)^{1/5} \times f(e)^{1/5}\left(\frac{r_0}{r_0+R}\right)^{1/20}\left(\frac{\rho V_0^2}{E}\right)^{1/20}.$$

If the adhesion energy is lower than the kinetic energy of the particle, $AR/6\varepsilon \ll mV_0^2/2$, then the van der Waals forces can be neglected. For this case, with head-on collision, we obtain a scalar equation for the gap between the particle and the fiber, $s_1 = [(R+r_0)/V_0T - |x' - \xi'|]$, which is dependent on only parameter λ_c:

$$\frac{ds_1}{d\tau} = 1 - \int_0^\tau \left[1 + \frac{\lambda_c}{(\tau-\tau')^{1/2}}\right]s_1(\tau')^{3/2}d\tau'. \quad (33)$$

Equation (33) differs from the corresponding equation derived for the case of the particle-plate collision [12]. The origin of the difference is related to different dimensions of the fiber and the plate. At zero time, $s_1(0) = 0$, $\dot{s}_1 = 1$. The collision is over when $s_1(\tau_k)$ reaches zero again.

Define the coefficient of restitution e_c as the ratio of the relative velocity after and before an impact:

$$e_c \equiv \frac{V_k}{V_0} = -\frac{ds_1(\tau_k)}{d\tau}. \quad (34)$$

The particle velocity upon impact in the laboratory frame of reference is

$$\frac{V(\tau_k)}{V_0} = -1 + \int_0^{\tau_k} s_1(\tau')^{3/2}d\tau'. \quad (35)$$

The dependence of the coefficient of restitution e_c on parameter λ_c was numerically calculated. For $0 < \lambda_c < 1$, the function $e_c(\lambda_c)$ is well approximated by

$$e_c = \exp\left(-1.781\lambda_c + 0.753\lambda_c^2 - 0.452\lambda_c^3\right). \quad (36)$$

Although Eq. (36) was derived for a head-on collision, in the no-friction case, it is also valid for an arbitrary shooting distance only if the λ_c parameter is determined by the radial component of the velocity. It should be noted that for $\lambda_c > 0.5$ the particle and the fiber move in the same direction after the collision, such that a complex dynamics of multiple collisions may occur. This is possible, e.g., for large particles, for which $R/r_0 \gg 1$. A simplified system of equations describing multiple collisions is given in Appendix B.

III. CRITICAL VELOCITY OF FLOW OF HEAVY AEROSOLS AT HIGH STOKES NUMBERS

In this section, using Eq. (36), we compare simple estimates for the critical velocity, which distinguishes the region of deposition of a moving particle from the region of rebound, with the computations by using the complete system of Eqs. (25)–(29) at $\mathrm{St} \gg 1$. The filtration of gas with aerosol particles of a size smaller than or of the order of 1 μm is often performed by pumping the air through a porous medium consisting of fibers with hydrodynamic resistance directly proportional to the flow velocity. As noted in the Introduction, the filtration process is usually conducted at small velocities, with the aim of lowering the gas flow resistance. Usually, for particles having a low density, the Stokes number is $\mathrm{St} \leqslant 1$. In this case one has to know the flow field near fibers to simulate the deposition of particles on a fiber. However, when the Stokes number is high, $\mathrm{St} \gg 1$, the influence of the gas flow field on the particle near the fiber surface can be neglected. The computation of the fiber collection efficiency in this limit is reduced to the computation of the trajectory of the particle motion as a function of the shooting parameter.

As an example, we investigate the high-velocity regime of deposition of submicron particles of heavy metals in fine-fibrous analytical filters. Consider the case of a filter with fine glass fibers with a diameter of 2 μm subjected to uniform flow with a velocity of 20 cm/s. For the elastic properties of the glass and aerosol particles, we assume that $E = E' = 10^{12}$ erg/cm^3, $\sigma = \sigma' = 0.3$. Hamaker's constant A is assumed to be equal to 10^{-12} erg, and the length of the fiber is $L = 100\,r_0$. For a particle with radius $R = 0.3$ μm, density $\tilde{\rho} = 10$ g/cm^3, and mass $m = 1.13 \times 10^{-12}$ g, the estimated collision time is $T = 1.35 \times 10^{-9}$ s, while the corresponding ratio of the

potential to kinetic energies and the parameters St, ωT, and $\tilde{\omega} T$ are

$$\frac{U_p}{W} = \frac{2AR}{6\varepsilon m V_0^2} = 0.5, \quad \mathrm{St} = 2.22,$$

$$\omega_1 T = 4.7 \times 10^{-3}, \quad \tilde{\omega}_1 T = 0.3.$$

In order to estimate the probability of an aerosol particle being captured by a fiber, one can use the limit of an infinitely long fiber. In this limit we can use the results of the computations of the restitution coefficient given by Eq. (36), and assuming that the coefficient of restitution is close to unity, the parameter λ_c is calculated from the minimal velocity of impaction $V = (2U_p/m)^{1/2}$ to be equal to $\lambda_c = 1.58 \times 10^{-2}$. According to Eq. (36), the corresponding restitution coefficient is $e_c = 0.97$.

For the capture of a particle by a fiber, neglecting friction, the following condition for the particle velocity applies:

$$V_0 < \left(\frac{2U_p}{m}\right)^{1/2} \left(\frac{1-e_c^2}{e_c^2}\right)^{1/2} \left[1 + \frac{b^2}{r_0^2 e_c^2}\left(1-e_c^2\right)\right]^{-1/2},$$

where b is the shooting distance. At the head-on collision of particles with $R = 0.3$ μm with a fiber, the velocity is estimated as $V_0 < 3$ cm/s. Thus, the collection of heavy particles of a given size at common sampling velocities may be noneffective. For particles having considerably smaller size at $V_0 = 20$ cm/s, the Stokes number is small, $\mathrm{St} \ll 1$, and the contact interaction of the particle and the fiber has a weak effect on the filtration efficiency.

Similar computations for a particle with $R = 1$ μm give $T = 4.68 \times 10^{-9}$s, $U_p/W = 0.035$, $\mathrm{St} = 24.7$, $\omega_1 T = 1.6 \times 10^{-2}$, $\tilde{\omega}_1 T = 0.65$, $\lambda_c = 0.33$. For deposition of the particle on the fiber to occur, the velocity must be limited to $V_0 < 5$ cm/s. It should be noted that for larger particles the limit for the velocity is higher since the parameter λ_c is greater. In this case the restitution coefficient e_c is smaller, and the energy losses due to emission of the transverse waves are greater.

We shall compare the obtained estimates for the critical velocity of deposition with the results of computations on the basis of the complete system of Eqs. (25)–(29), describing the interaction between the aerosol particle and the fiber. Shown in Figs. 4 and 5 are dependencies for the particle velocity components V_x, V_y for the gap between the particle and the fiber s and for the stress σ versus dimensionless time at the particle-fiber collision. The initial position of particles was chosen at large positive values of the x coordinates and at dimensionless shooting distance $y = b/(R + r_0)$. The initial particle velocity V_0 was directed along the x axis toward the fiber, which was placed in the origin. In Fig. 4 our computational results are illustrated for two values of initial velocity for a particle with a radius of 0.3 μm. In Fig. 5 the results of similar computations for a particle with a radius of 1 μm are presented.

Figure 4(a) illustrates the particle velocity dynamics in the region near a fiber: acceleration of a particle with an initial velocity of 1 cm/s in the fiber direction due to the action of the attractive van der Waals force before the moment of collision, the rapid change of the velocity direction due to the action of elastic forces at contact, and the same velocity change until the second collision. The dependence of the gap s versus time is illustrated in Fig. 4(b). The maximum value of the gap decreases from collision to collision (only two are shown) because of the energy losses upon contact. Particles were eventually captured after many collisions. It should be noted that the gap value becomes negative at the very moment of the contact of the particle with the fiber. The corresponding elastic stresses are shown in Fig. 4(c). In Figs. 4(d)–4(f), similar curves are shown for a velocity of 5 cm/s for which the particle returns to the stream after a single collision.

For particles of a larger size having a radius of 1 μm, moving toward the fiber with a velocity of 3 cm/s, the dynamics of the process is shown in Figs. 5(a)–5(c), where the gap s gradually tends to zero. For a high velocity of 6 cm/s a single collision occurs, and a particle returns to a stream. From Fig. 4 it follows that a particle with a radius of 0.3 μm should deposit on the fiber if the initial velocity is 1 cm/s, while at 5 cm/s the particle should miss the fiber after a single collision. Thus, one can see that the critical velocity of deposition on the fiber for heavy particles with a radius of 0.3 μm lies within the interval 1 cm/s $< V^* <$ 5 cm/s, while for particles with a radius of 1 μm the interval is 3 cm/s $< V^* <$ 6 cm/s. The predictions for the velocity of the particle deposition on the basis of Eq. (36) agree with the results of computations with the full system of Eqs. (25)–(29).

The results of the computations for a particle with radius 1 μm and initial velocity 20 cm/s are given in Fig. 6. This is a typical face flow velocity for sampling with analytical filters. Figure 6(b) shows the time dependence of the gap s. From this plot one can see that heavy particles do not deposit at the given conditions. In Fig. 6, with plots similar to those in Figs. 4 and 5, the time dependencies are shown for the angular rotational velocity of the particle ω_0 [Fig. 6(d)] and for the fiber at the point of contact ω [Fig. 6(e)], as well as for the translational kinetic energy $W_t = mV^2/2$ and overall kinetic energy of the particle during the process of collision [Fig. 6(c)].

We call attention to the fact that the angular velocity of a fiber in the point of impact is an antisymmetric function $\omega(t + t_1) = -\omega(t)$ with a period t_1 equal to the time of flight of elastic torsional waves over the whole length $t_1 = L/\tilde{\beta}_c$. This is consistent with the analysis given in the Appendix A. The computations were performed for 50 harmonics and for the friction coefficient $k_t = 0.3$.

It is also interesting to trace the deformation of the fiber form after the collision. Different forms of a fiber with $r_0 = 1$ μm at intervals of time are shown in Fig. 7(a) for the case of the head-on collision with a particle with $R = 1$ μm and initial velocity of 20 cm/s. It is seen that the perturbation has no time to reach the end point of the fiber, and thus, the approximation of the infinite fiber is valid. The dependence of the location of the middle of a fiber versus time is shown in Fig. 7(b). Arrows at the time axis correspond to the onset and the end of the contact interaction. After the collision, the fiber continues to deform until the perturbation reaches the fixed ends of a fiber. The difference between the behavior of deformation after the collision of a particle with an infinite fiber and with an infinite plate is discussed in full detail in Appendix A.

So far, all dissipative processes have been neglected. Below, the range of validity of this assumption will be

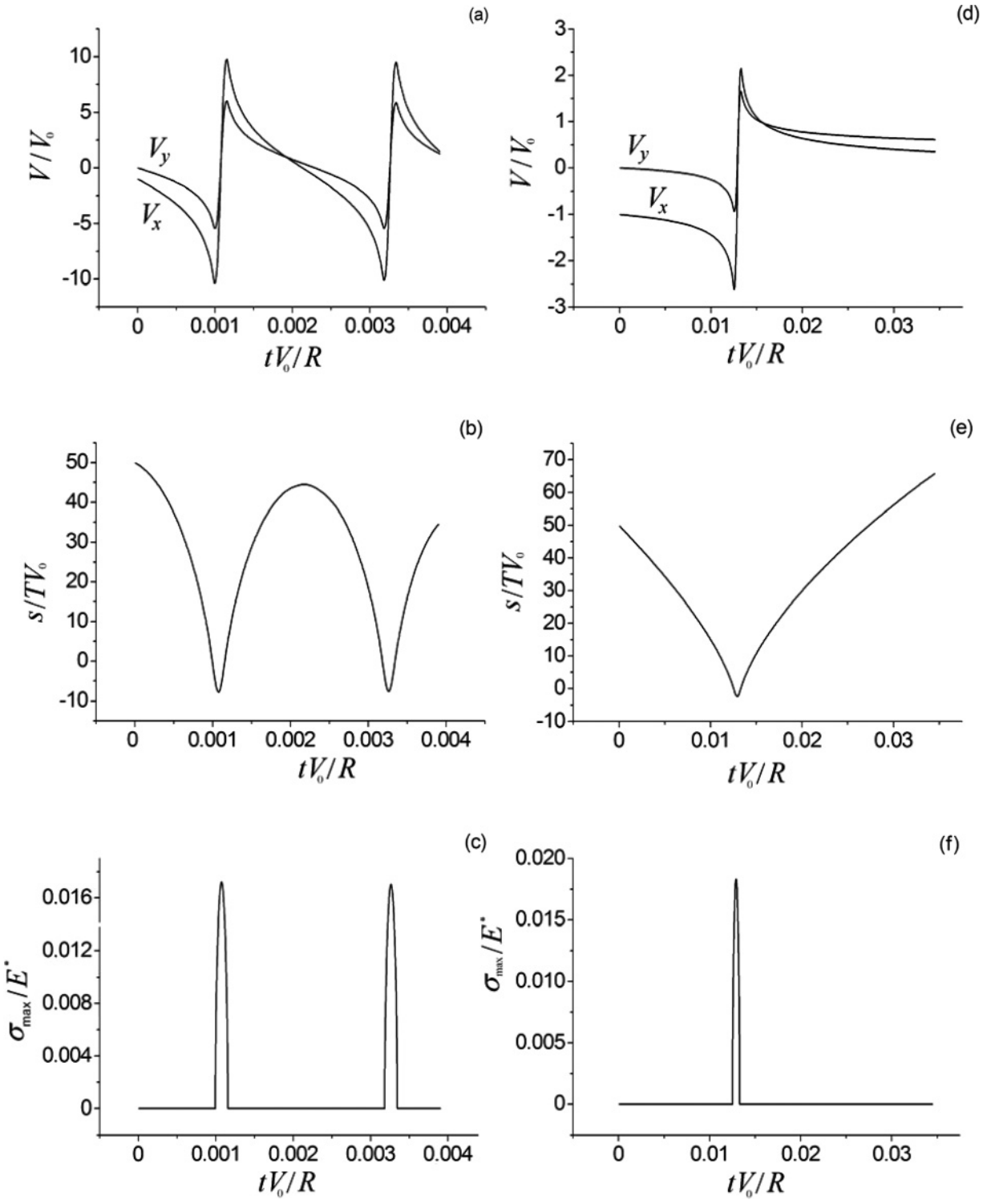

FIG. 4. (a, d) The velocity components, (b, e) the gap, and (c, f) the maximal stress vs time at the collision of a particle with radius $R = 0.3$ μm with a fiber with radius $r_0 = 1$ μm for two values of the face flow velocity (a−c) $U_0 = 1$ cm/s and (d−f) $U_0 = 5$ cm/s, with dimensionless shooting parameter $y = 0.5$.

estimated. For high-velocity impacting particles, two regimes may occur, depending on the nature of the material of the interacting bodies: plastic deformation or the formation of microcracks in brittle particles and fibers, with their subsequent failure. The maximal stresses of compression at the collision occur on the surface in the center of the contact region [16,18]:

$$\sigma_{\max} = \frac{2}{\pi}\frac{E^{*4/5}}{R^{3/5}}\left(\frac{15}{16}mV_0^2\right)^{1/5}. \tag{37}$$

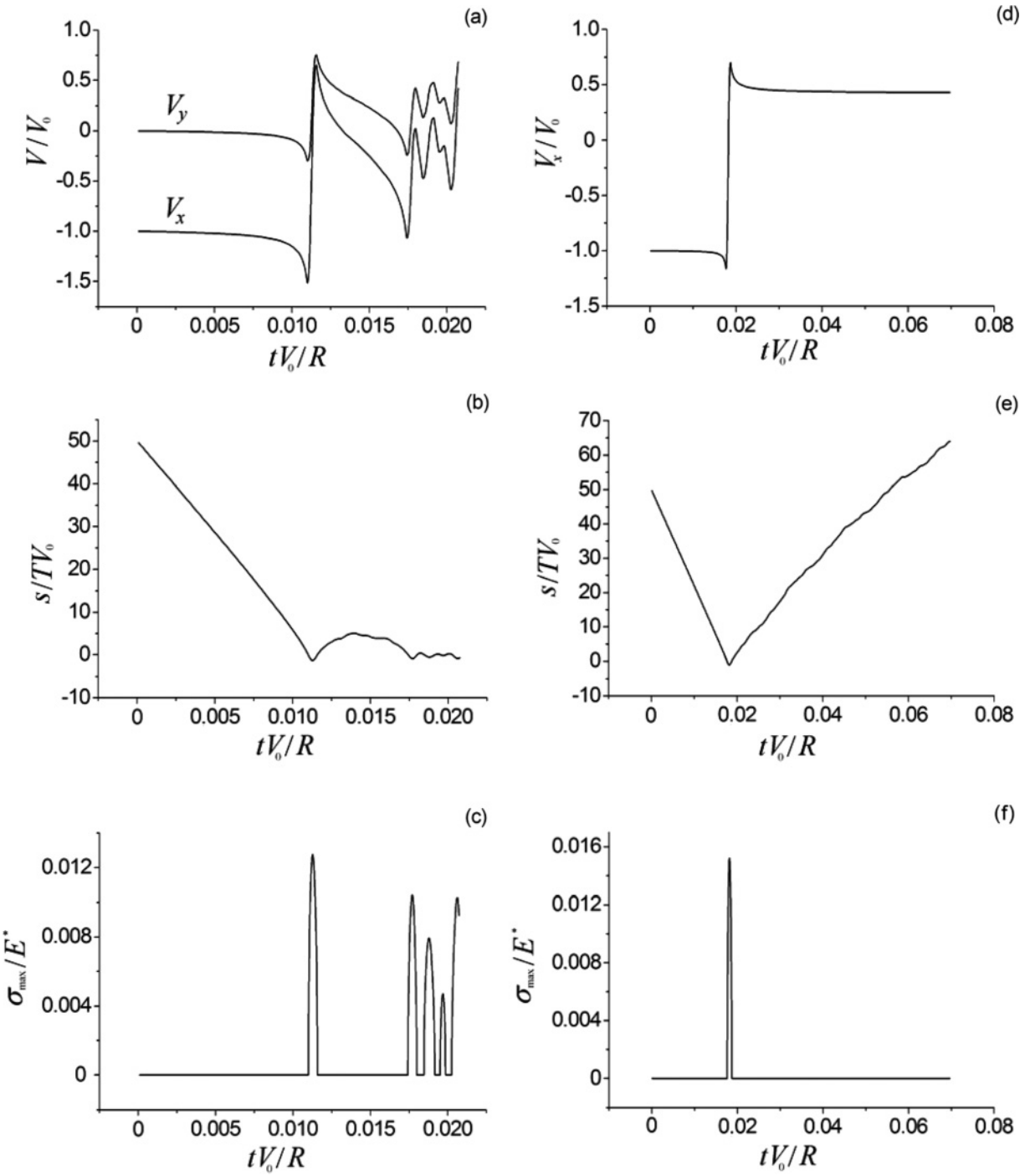

FIG. 5. (a, d) The velocity components, (b, e) the gap, and (c, f) the maximal stress vs time at the collision of the particle with radius $R = 1$ μm with the fiber with radius $r_0 = 1$ μm for two values of the face flow velocity (a−c) $U_0 = 3$ cm/s and (d−f) $U_0 = 6$ cm/s, with dimensionless shooting parameter (a, b, c) $y = 0.5$ and (d, e, f) $y = 0$.

These stresses do not exceed the failure threshold for brittle materials σ_b at velocities lower than the critical value:

$$V_0 < \left(\frac{\pi^4}{40}\right)^{1/2}\left(\frac{E^*}{\tilde{\rho}}\right)^{1/2}\left(\frac{\sigma_b}{E^*}\right)^{5/2} = \left(\frac{\pi^4}{40}\right)^{1/2}\left(\frac{E}{\tilde{\rho}}\right)^{1/2}\left(\frac{\sigma_b}{E}\right)^{5/2}\left(\frac{E}{E^*}\right)^{2}. \quad (38)$$

For glassy fibers for which $E \approx 4 \times 10^{12}$ erg/cm^3 and $\sigma_b/E \approx 10^{-2}$, the estimation $V_0 < 30$ cm/s for the critical velocity is obtained, provided that the elastic moduli of the fiber and the particle are of the same order. For plastic materials the losses due to plastic deformation can be estimated as in [14].

Another channel of the dissipative processes is connected to hysteresis losses due to deformation of the impacting particle

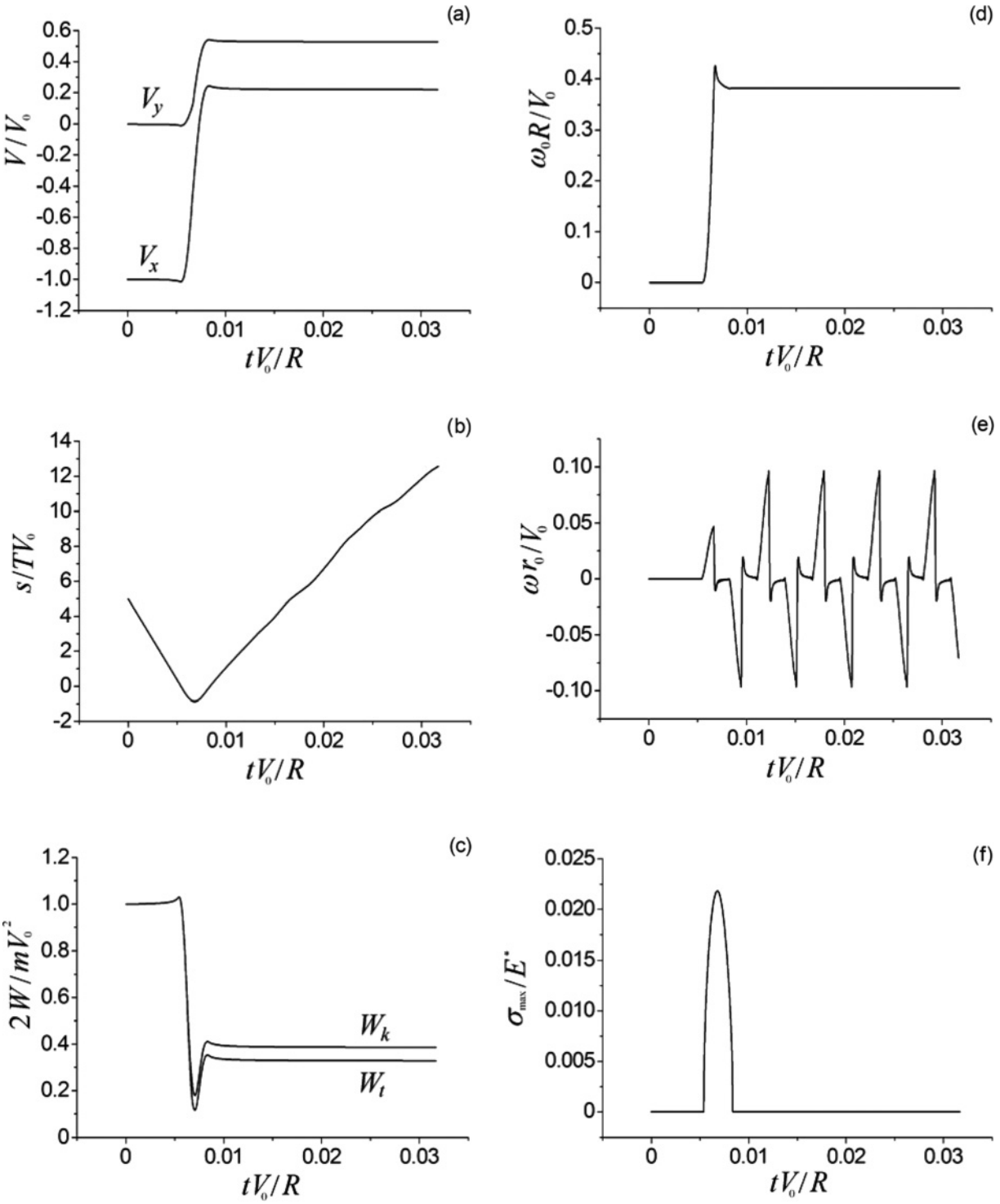

FIG. 6. (a) The particle velocity components, (b) the gap, (c) the translational and overall kinetic energy of the particle, (d, e) the angular velocity of the particle and the fiber, and (f) the maximal stress vs time at the high-velocity impact of the particle on the fiber, with $U_0 = 20$ cm/s and dimensionless shooting parameter $y = 0.5$.

with van der Waals' forces. According to the Johnson-Kendall-Roberts theory [19], the force of interaction F and the relative displacement δ are given in terms of the radius of the contact zone a by

$$F = \frac{4E^*}{3R}a^3 - 4E^*(\pi\tilde{r})^{1/2}a^{3/2}, \tag{39}$$

$$\delta = \frac{a^2}{R} - (4\pi\tilde{r}a)^{1/2}, \tag{40}$$

where the radius $\tilde{r}$ is related to the surface tension γ of the particle,

$$\tilde{r} \equiv \frac{\gamma}{E^*}.$$

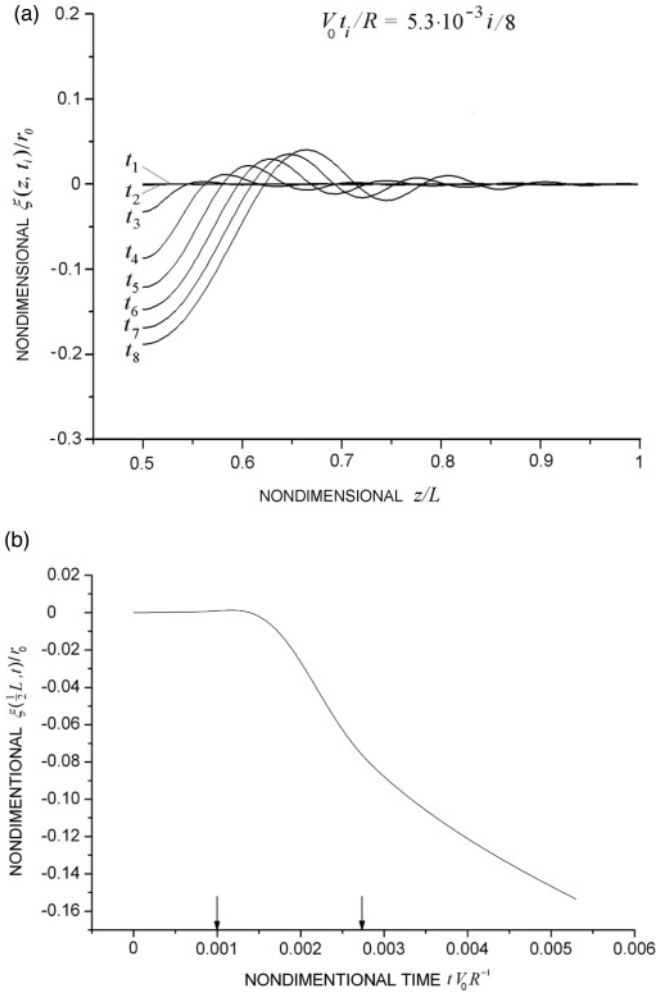

FIG. 7. (a) The form of the fiber varied due to interaction with a fast particle at several subsequent values of time and (b) the time dependence of the displacement of the fiber-particle contact point at $z = L/2$. Arrows denote the onset and the end of the particle-fiber contact interaction.

The surface tension γ can be expressed in terms of Hamaker's constant,

$$\gamma = \frac{A}{12\pi\varepsilon^2}.$$

For the interval $0 < a < R(\pi\tilde{r}/4R)^{1/3}$ the function $F(\delta)$ is two-valued. This leads to different interaction potentials between the particle and the fiber at the compression and rebound stages, which, in turn, leads to adhesion losses.

Hysteresis losses will be governed by the work done by the force $F(\delta)$ over the region of two-valuedness:

$$W_a = \int_0^{a_p} F(a)\frac{d\delta}{da}da.$$

By evaluating this integral, we find the adhesion losses

$$W_a = 3.2E^*R^3\left(\frac{\pi\gamma}{4E^*R}\right)^{5/3}. \tag{41}$$

The theory [19] is valid when parameter μ_1, first introduced in [20], is large enough,

$$\mu_1 = \left(\frac{\gamma^2 R}{E^{*2}\varepsilon^3}\right)^{1/3} \gg 1. \tag{42}$$

The particle deformation due to the action of dispersion forces was first considered in [21]. Later computations can be found in [22]. In these works, it was shown that for $\mu_1 \leqslant 1$ the losses due to hysteresis are small or absent. For the aerosol particles under consideration here, the mentioned parameter is equal to $\mu_1 = 0.05$ for $R = 0.3\mu$m, while for a particle with $R = 1\mu$m one obtains $\mu_1 = 0.075$. Therefore, the hysteresis losses of energy should be small. Thus, at typical operational flow velocities smaller than 10 cm/s for heavy aerosol particles with $\mathrm{St} \gg 1$, the basic losses of energy upon collision of particles with fibers are those due to the excitation of elastic fiber vibrations. The dissipative losses can also be connected to the friction exerted by a gas on a fiber and a particle at low Stokes numbers.

IV. COMPUTATION OF THE FILTER COLLECTION EFFICIENCY DUE TO THE INERTIA OF PARTICLES WITH St ~ 1

In this section we present the results of simulations for the deposition of aerosol particles on fibers of a filter for moderate gas flow velocities based on Eq. (36) for the coefficient of restitution. In the gas filtration literature there exist a large number of empirical formulas for predicting the efficiency of filtration in the inertial regime at different conditions [23]. But there have been no computations performed from first principles that considered both the movement of the particle in the gas stream due to attractive forces and the rebound of the particle from the fiber surface upon contact.

A fibrous filter is usually a highly porous thin layer of material consisting of randomly arranged long fibers. The actual flow field is difficult to predict, as the correlations between fibers are not known. Therefore, the average flow field is often used in the vicinity of fibers. For a single fiber in a random fibrous medium and an averaging procedure with respect to the coordinates and orientations of all other fibers, a two-dimensional flow field will result. Different models are used to represent the influence of the neighbor fibers on this average flow field [1]. An example is the model of the transverse flow past a periodic hexagonal lattice of parallel fibers.

Further simplification was suggested in [24]. This model describes well the dependence of the hydrodynamic resistance of the hexagonal lattice versus packing density α at small flow velocities. It is worth noting that plane flows are often used in experiments for investigating the deposition of particles upon a single fiber or a row of parallel fibers [1,4,23]. In addition to the average flow field, there would be fluctuating velocities caused by the neighboring fibers. For a low fiber packing density α the average distance cut by the neighbor fibers on the given fiber will be of the order of $r_0/\alpha \gg r_0$, which is easily seen if, for instance, the fibers in the nearest layers form a square lattice in the plane of the filter. Hydrodynamic perturbations initiated from the fiber intersections propagate to a distance of the order of the fiber radius, as in the case

of the flow past a sphere. At small packing densities α, these perturbations would have a small effect on the particle deposition since the fraction of these regions of perturbations is of order α. Thus, the size of the fluctuating fields should be of the order r_0/α. At such large scales at St ~ 1 the particle inertia should be negligible. The particles are expected to move following streamlines with constant concentration since the gas flow is considered as incompressible. It may be that the inhomogeneity of the flow along the fiber length is the main effect of the long-wave velocity fluctuations on the filtration efficiency. We will first investigate the deposition of particles on a fiber in a plane transwerse flow, and then the influence of the flow inhomogeneity along the fiber length is estimated.

The simulations were performed for the Stokes flow in a fibrous filter, for which the nondimensional stream function $\Psi(r,\varphi)$ and the corresponding components of the flow velocity found by Kuwabara in the framework of the cell model [24] were used:

$$\Psi(r,\varphi) = \frac{1}{K_1}\sin(\varphi)\left(\frac{2-\alpha}{4r}+\frac{\alpha-1}{2}r+r\ln r-\frac{\alpha}{4}r^3\right), \tag{43}$$

$$U_r = -\frac{\partial\Psi}{r\partial\varphi},\ U_\varphi = \frac{\partial\Psi}{\partial r}.$$

Here α is the packing density of fibers in the filter (volume of fibers per unit volume of filter), and $K_1 = -0.5\ln\alpha - 0.75 + \alpha - 0.25\alpha^2$ is the hydrodynamic factor. Our simulations were performed for $\alpha = 0.05$. In Eq. (43) the distances are normalized with r_0 and velocities with U_0. The particle trajectories were found from the system of nondimensional equations with van der Waals and particle drag forces:

$$\begin{aligned}\frac{dV_r}{dt} &= \frac{V_\varphi^2}{r} - \frac{1}{\mathrm{St}}(V_r - U_r) + F_r\frac{r_0}{mU_0^2},\\ \frac{dV_\varphi}{dt} &= -\frac{V_r V_\varphi}{r} - \frac{1}{\mathrm{St}}(V_\varphi - U_\varphi).\end{aligned} \tag{44}$$

A method of computation of the van der Waals forces at distances $s \gg \varepsilon$ is given in Appendix C. The particles were launched from the cell boundary at the radius $r = \alpha^{-1/2}$, with an initial velocity equal to the gas flow velocity $\mathbf{V} = \mathbf{U}$. The van der Waals force was defined as a piecewise function (see Appendix C). Equations (44) were solved by the finite-difference scheme of Runge-Kutta-Fehlberg of order 4–5 [25].

Examples of the trajectories are given in Fig. 8(a) for particles with radius $R = 0.3$ μm and for low flow velocities. They were computed with completely elastic particle-fiber collisions. Even for perfectly elastic collisions, all particles that touch the fiber will deposit on it. The losses of energy of a particle are connected with the gas friction during its vibrative motions near the fiber. Shaded areas in Figs. 8(a) and 8(b) depict the regions on the fiber surface in which the particles, after collision with the fiber, are eventually captured.

At Stokes numbers lower than critical, the collision of the particle with the fiber results in particle deposition. At Stokes numbers higher than the critical value [see Fig. 8(b)] and at $R/r_0 < 1$, there are two regions (zones) of deposition surrounding a region in which all rebounded particles

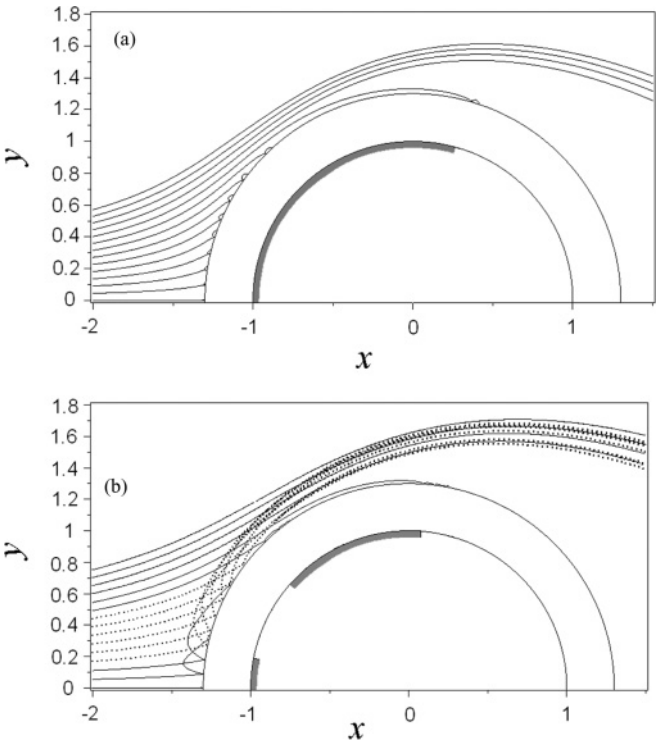

FIG. 8. Examples of simulated trajectories for particles with radius $R = 0.3$ μm for the face flow velocities (a) $U_0 = 5$ cm/s and (b) $U_0 = 8$ cm/s. The fiber packing density is $\alpha = 0.05$, the fiber radius is $r_0 = 1$ μm, and the particle density is $\tilde{\rho} = 10$ g/cm^3.

eventually leave the fiber. In the first zone of deposition, in the vicinity of the axis of symmetry, head-on collisions take place, followed by rebounds with reduced velocity. The second zone of deposition is found close to 90°. Thus, in the upper semiplane, there is not one, but three, limiting trajectories. The fiber collection efficiency η is defined as the ratio of the number of particles depositing on the fiber unit length in a unit of time to the flux $2r_0U_0n_0$, where n_0 is the particle concentration in a stream. The fiber collection efficiency η is an important quantity in the theory of filtration as it defines the coefficient of penetration of particles P, which, in turn, governs the efficiency of filtration. The particle penetration P is equal to the ratio of the flux of particles that passed through the filter to the inlet flux. It is given by the formula $P = \exp(-2\eta\alpha H/\pi r_0)$, where α is the filter packing density and H is the filter thickness [1]. In the case of a single limiting trajectory the fiber collection efficiency η is equal to the value of the dimensionless stream function Ψ_1 at the initial point of the limiting trajectory at the cell boundary. For the case when the rebounded particles appear, the fiber collection efficiency is found as $\Psi_1 - \Psi_2 + \Psi_3$, where the stream functions Ψ_i are governed by the limiting trajectories, starting with those that are the most distant from the stream symmetry plane.

The calculated dependence for η is given in Fig. 9 for different coefficients of restitution versus the face flow velocity at low Stokes numbers. In Fig. 9, curve A was plotted for the case of full adhesion at $e_c = 0$. A feature of curve A can be easily explained. Neglecting attractive forces in the region of low Stokes numbers, a particle follows a streamline and

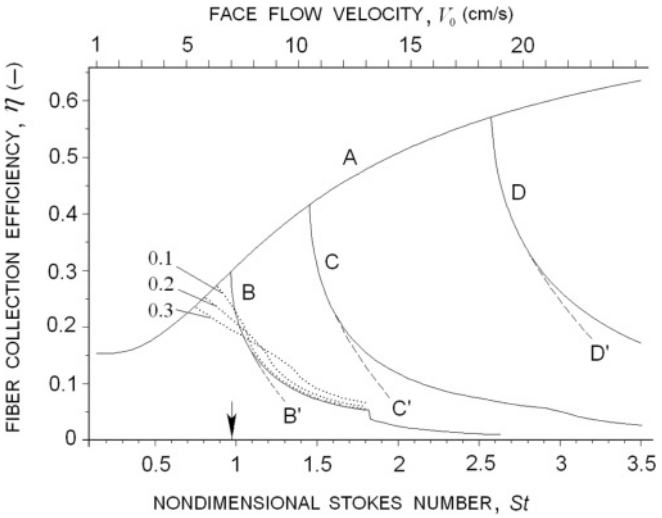

FIG. 9. Fiber collection efficiency vs Stokes number (velocity U_0) plotted for inertial particles with radius $R = 0.3$ μm and for a fiber with radius $r_0 = 1$ μm in a filter with packing density $\alpha = 0.05$, accounting for the rebound of particles for different coefficients of restitution e_c. Curve A, no rebound ($e_c = 0$); B, $e_c = 1$; C, e_c defined by Eq. (36); D, $e_c = 0.8$. The dashed curves B′, C′, and D′ correspond to simple approximations described in the text. Dotted curves correspond to the fiber collection efficiency for $e_c = 1$ averaged over the fiber length for nonhomogeneous flow varying along the fiber length by the formula $U(z) = U_0[1 + \varepsilon_1 \sin(kz)]$ for three values of perturbation ε_1 (given on curves).

deposits only if the streamline is closer to the fiber than the particle radius. With attractive forces and inertia, the particle is pulled from the streamline toward the fiber, resulting in an increase in the collection efficiency. The influence of the particle inertia increases with stream velocity, and, in the limit of high velocities, when $\mathrm{St} \gg 1$, the particle moves almost along a straight line due to inertia, and the fiber collection efficiency reaches its limit, $\eta = (R + r_0)/r_0$.

Curve B corresponds to the case of full rebound (bounce off) at the coefficient of restitution $e_c = 1$. Also shown is the dependence for the coefficient of restitution e_c defined by Eq. (36) (curve C). Curve D corresponds to $e_c = 0.8$. There is a rapid decrease in the fiber collection efficiency with increasing face flow velocity (Stokes number). This behavior is explained by particles that escape after two rebounds. Other curve cusps may appear with the rise in the Stokes number due to particles escaping fibers with a large number of rebounds. The dashed curves B′, C′, and D′ are simple approximations of the form $\eta = \eta_0 - a(\mathrm{St} - \mathrm{St}_0)^{1/2}$, where a is the coefficient of approximation and the subscript 0 corresponds to the critical Stokes number, which is related to the cusp appearance. The calculated fiber collection efficiencies are well described by the square-root dependence at Stokes numbers slightly higher than the critical value.

It is seen from Fig. 9 that there is a minimal critical velocity or a minimal critical Stokes number, below which even an elastic interaction of particles with a fiber surface does not lead to a decrease in the filtration efficiency. The critical value of the Stokes number is a function of all dimensionless parameters defining the movement of aerosol particles:

$$\mathrm{St} = f\left(\frac{A}{mU_0^2}, \frac{R}{r_0}, \alpha, \ldots\right). \tag{45}$$

When the velocity is greater than the minimal critical velocity, the filtration efficiency is determined by the mechanism of the particle energy loss at the collision and may become much lower. The minimal critical value of St is depicted by an arrow in Fig. 9.

The computations performed show the presence of cusps on the η-U curves. However, no sharp cusps are observed in experiments, which can be explained by the polydispersity of aerosol particles and fibers, by a variable gas flow along the fiber length, and by time fluctuations of the velocity. We expect that averages over all of these parameters will result in smoothed curves. As an illustration, in Fig. 9 the dotted curves denote the dependencies of the fiber collection efficiency for $e_c = 1$, averaged over the fiber length with the assumption that the velocity is varied along the fiber in accordance with the law $U(z) = U_0[1 + \varepsilon_1 \sin(kz)]$. The increased flow inhomogeneity at higher ε_1 values leads to less-inclined curves at the cusp points.

We have theoretically investigated the interaction of solid heavy particles with fine fibers when the basic inelastic losses are due to excitation of long-wave elastic vibrations in the fibers. We are not aware of any specific experiments with heavy aerosol particles. The majority of experiments have been conducted with polystyrene particles. Our results can be formulated on the basis of Fig. 9. At small Stokes numbers St the fiber collection efficiency should always follow curve A, with $e_c = 0$. There exists a critical velocity that, for elastic collisions at $e_c = 1$, governs the appearance of rebounded particles that return to the stream. When the stream velocity is greater than the critical value, the fiber collection efficiency is affected by various inelastic processes. The greater the inelastic losses during collision are and, correspondingly, the smaller the coefficient of restitution $e_c$is, the higher the Stokes numbers will be that correspond to the onset of deviation of the curve $\eta(\mathrm{St})$ from curve A, as seen from curves C and D.

Finally, we compare the obtained results with recently reported experimental data [23]. The comparison is only qualitative since, for numerical agreement, one has to perform computations for conditions of the given experiment, as the inertial deposition is sensitive to the flow field, properties of the particle and fiber materials, their size, and the condition of their surface. First of all, it should be noted that in the cited study the Stokes number was defined by the fiber diameter, while we have defined it by its radius. Therefore, the results differ twofold. We follow our definition. The experiment was conducted with polystyrene particles with radii of 1.3 and 2.6 μm depositing upon a single fiber. In experiment, a maximum in the fiber collection efficiency was seen at $\mathrm{St} \sim 4$ for 1.3 -μm particles (at $U_0 \sim 120$ cm/s) and at $\mathrm{St} \sim 6$ for 2.6-μm particles at a flow velocity of the order of 50 cm/s. For large particles the maximum on the curve $\eta(\mathrm{St})$ should be higher. This is explained as follows: the particle trajectories are the same at the same Stokes numbers while neglecting the attractive forces, but particles with greater size are able to reach

the fiber faster. Equation (36) shows that for the fibers used in the experiment the shown radiation losses are negligible. Here the losses can be estimated in a way similar to the case of the interaction with the plane. Adhesion losses are estimated by Eq. (41). The material properties are as given in [14]. The surface tensions of steel and polystyrene are $\gamma_s = 1.62$ J/m^2 and $\gamma_P = 0.03$ J/m^2; values of the modulus of elasticity are given by $E_s = 190$ GPa, $E_p = 3$ GPa. If $E_s \gg E_p$, then $E^* \sim E_p$. For estimations we assume that $\gamma = \gamma_s$. Inserting these values into the formula for the energy dissipation due to hysteresis [Eq. (41)] and expressing the restitution coefficient e_c in terms of the adhesion losses $e_c = (1 - 2W_a/mV_0^2)^{1/2}$, we obtain the following estimate for the coefficient of restitution:

$$e_c = \left(1 - B\frac{R^{7/3}}{r_0^2 \mathrm{St}^2}\right)^{1/2},$$

where the coefficient B is independent of the geometric dimensions.

For particles with a radius of 1.3 μm at St ~ 4 we obtain $e_c = 0.95$, while for particles with a radius of 2.6 μm at St ~ 6 the coefficient of restitution is $e_c = 0.89$. If the given estimates are not significantly changed by the losses of energy due to plastic deformations, then the decrease in e_c with the particle radius increase explains the occurrence of the maximum in the dependence of the fiber collection efficiency at high Stokes numbers for particles with large radii.

V. INFLUENCE OF FILTER PACKING DENSITY ON EFFICIENCY OF FILTRATION

In a sufficiently dense fibrous medium the rebounded particles at high Stokes numbers may not attain the flow velocity U_0 during the time between the collisions. We assume the fibrous medium to consist of a number of touching flat layers, where every layer is formed by an entity of random, independent, infinitely long straight fibers arranged in these layers. Let us consider a circumference of radius $R_1 = R + r_0$ that belongs to one of the layers. Random fibers will cross this circumference. The average length of segments $\bar{l}$ that is cut from random fibers by this circumference is equal to [26]

$$\bar{l} = \frac{\pi}{2}(R + r_0).$$

The total length of all of the fiber segments cut by the circumference is $\bar{l}N$, where N is an average number of fibers crossing the considered circumference. Equating the ratio of the volume of all of the fibers $N\bar{l}\pi r_0^2$, crossing the circumference to the volume of the layer of a filter with the surface area $\pi(R + r_0)^2$ and the thickness $2r_0$, to the packing density α, we express the average number of fibers N in terms of α:

$$N = \frac{4\alpha(R + r_0)}{\pi r_0}.$$

Since the fibers are independent, the probability of the intersection of the considered circumference with n fibers is governed by Poisson's distribution,

$$P_0(n) = \frac{N^n}{n!}e^{-N}.$$

Next, estimate an average length $\bar{l}_1$ of the flight of the particle along the straight line perpendicular to the filter surface before the collision with the fiber. For this purpose the average number of fibers from $\bar{l}_1/(2r_0)$ layers, projected to a single surface and intersecting the circumference with radius $R + r_0$, must be of order unity. We assume that the transverse cross section of the particle is crossed by two fibers,

$$\frac{\bar{l}_1}{2r_0}N = \frac{\bar{l}_1 4\alpha(R + r_0)}{2\pi r_0^2} = 2,$$

from which the estimate for the length $\bar{l}_1$ is found:

$$\bar{l}_1 = \frac{\pi r_0^2}{\alpha(R + r_0)}.$$

Now estimate the length at which the initially motionless particle attains the stream velocity U_0. From the equation of motion of the particle at low velocities we find the time of acceleration $t \sim m/6\pi\mu R$ and the corresponding length of acceleration $l \sim U_0 t = r_0\mathrm{St}$. A particle will not have time to accelerate to the stream velocity if $\bar{l}_1 \ll l$. This leads to the following condition for the Stokes number:

$$\frac{\pi}{\alpha}\frac{r_0}{R + r_0} \ll \mathrm{St}. \tag{46}$$

In this case, in order to estimate the filtration efficiency, one has to know the particle velocity distribution. The computation of the coefficient of penetration of particles through the filter P was performed with the Monte Carlo method. A simple model was proposed. The particles are moving between collisions in the field of the constant hydrodynamic velocity $\mathbf{U}_0$. The particle velocity is varied in time in accordance with

$$\mathbf{V}(t) = \mathbf{U}_0 + (\mathbf{V}_1 - \mathbf{U}_0)\exp\left(-\frac{U_0 t}{r_0\mathrm{St}}\right). \tag{47}$$

Having passed a random distance l_1, which is uniformly distributed within the interval $0 < l_1 < \frac{2\pi}{\alpha}\frac{r_0^2}{R+r_0}$, the particles hit the fibers. As a result of the collision, the particle velocity deviates with equal probability for an arbitrary angle with a loss of part of the particle energy provided that the particle velocity is greater than the threshold value, or deposition on the fiber occurs.

The results of computations for the coefficient of the particle penetration through the filter P versus the filter packing density α are given in Fig. 10. The particle penetration P, as mentioned, is equal to the ratio of the flux of penetrated particles to the flux before the filter. Here the product of the thickness of the filter to the packing density is kept constant in order to keep the overall length of fibers in the filter volume. The following parameters were chosen: $H\alpha = 2.5 \times 10^{-3}$ cm, $U_0 = 20$ cm/s, $R = 0.5$ μm, $r_0 = 0.1$ μm, $m = 5.2 \times 10^{-12}$ g, and St $= 61.7$. The computations were performed for the two values of the coefficient of restitution $e_c = 0.9$ and $e_c = 0.5$. The threshold velocity was chosen to be equal to $0.2\,U_0$. The results of the simulations were averaged over 10^4 trajectories.

From Fig. 10 it is seen that the penetration curves fall steeply with the packing density. This result is somewhat unexpected for loose filters, but the very existence of this effect is possible, particularly, for aerosol particles of heavy metals. In the given example a very loose filter (remaining very porous at a several-fold compression) was chosen. Thus,

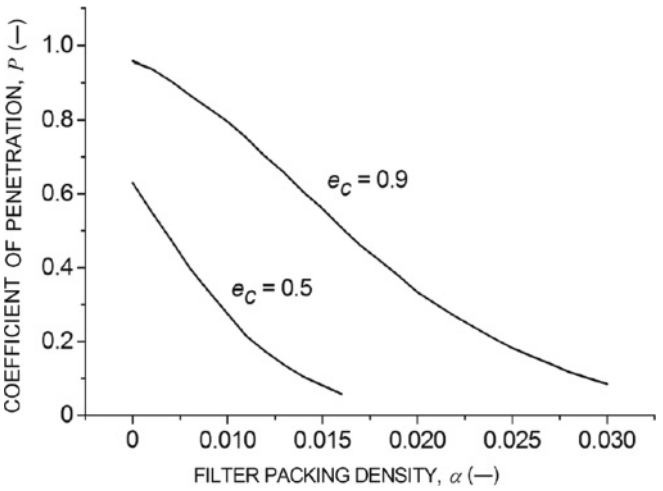

FIG. 10. Monte Carlo simulations for the coefficient of penetration of aerosol particles through the filter P vs the filter packing density α for two values of the restitution coefficient.

an infinitely small increase in the flow velocity within this filter should not affect its efficiency. Here the rise in the efficiency is explained only by the fact that the rebounded particles have no time to attain the velocity of the gas stream. Of course, the magnitude of the effect is dependent on the prescribed coefficient for the threshold velocity. For illustrative purposes, this coefficient was small since this is the case for particles with a high density of material. This effect complements the list of characteristic features of fine filtration of heavy aerosols. However, it should be noted that in the case of real filters with dense packing, $\alpha > 0.1$, further compression of a filter may lead to an increase in efficiency mainly due to the sieve effect, where the particle center goes between fibers with an interfiber distance smaller than the particle radius in some regions of the filter. The probability of the appearance of traps can be estimated in terms of the Poisson distribution for the number of fibers crossing the transverse cross section of the particle. For particle trapping, it is required that at least three fibers from a given or neighboring layers be within a radius of $(R + r_0)$. From this it follows that the probability for the particle to appear in the trap is of the order of $P_0(3) = \frac{N^3}{3!}e^{-3N}$ and, hence, is proportional to α^3 at small packing densities, $\alpha \ll 1$. Thus, one can infer that the presence of the considered traps should have little effect on the dependence of the coefficient of penetration of particles $P(\alpha)$ versus packing density at small values of α.

The condition (46) may be fulfilled for heavy particles. For example, Ref. [27] reports the experimental results with the following parameters: $R = 1.6\ \mu$m, $r_0 = 7.5\ \mu$m, $U_0 = 100$ cm/s, $\alpha = 0.033$, and $H = 0.6$ cm for particles with density $\tilde{\rho} = 7.8$ g/cm^3. The corresponding Stokes number was St $= 32$. The coefficient of penetration was $P = 0.4$, which is one order greater than estimated with the formula $P = \exp(-2\eta\alpha H/\pi r_0)$ with fiber collection efficiency $\eta \sim 0.2$, defined by inertial mechanism of deposition without rebound. In order to use the results obtained in this section, the stream velocity U_0 must be increased by a factor of 2.5, according to Eq. (46).

VI. CONCLUSIONS

The excitation of sound vibrations in fine fibers of a filter during the impaction of aerosol particles was studied. The equations describing the dynamics of impact were derived for an arbitrary shooting parameter. As shown, the losses of energy of a particle due to excitation of elastic waves may govern the efficiency of the particle deposition. It was shown that for long fibers the coefficient of restitution is a function of only parameter λ_c, which is defined by Eq. (32). The restitution coefficient was shown to be a function of the radial component of the particle velocity, the mass of a particle, the fiber density, the modulus of elasticity, and the geometric parameters of a fiber and a particle. The coefficient of restitution was calculated, and its analytical approximation was derived [see Eq. (36)].

The dependence of the filtration efficiency of the fibrous filter versus the face flow velocity was investigated. The existence of the critical face velocity was shown, below which the losses of energy during collision have no influence on the collection efficiency. For velocities higher than the critical value the filtration efficiency is dependent on the mechanisms of nonelastic losses of the particle energy. Its value can be significantly lower than that estimated by the theory of the full adhesion without accounting for the particle rebound effect.

At high flow velocities, rebounded particles appear. This leads to the velocity distribution for the particles in the stream. The particle velocity distribution and the fiber collection efficiency will be dependent on the fiber packing density α. As shown for a simple model, the filtration efficiency should increase with the packing density α at the constant value of the total fiber length per unit surface of the filter, $\alpha H = \text{const}$, and at high flow velocities.

The results obtained above illustrate the basic features of fine filtration of gas containing submicron suspended particles with a high density of a material. It follows from the presented results that the penetration of such particles through highly efficient fine-fibrous filters may occur at typical operational flow velocities.

ACKNOWLEDGMENTS

Authors thank an unknown referee for helpful comments. V.A.K. acknowledges support from the Russian Foundation for Basic Research (Project No. 10-08-01073a).

APPENDIX A: DEFORMATION OF AN INFINITE FIBER AS A RESULT OF INITIAL IMPACT

As a result of the collision of a particle with a fiber or a flat plate, the regions near the contact area attain an initial velocity and continue to deform after the collision. In this Appendix we show that the dynamics of deformation of an infinitely long one-dimensional fiber and that of a two-dimensional unbounded plate upon obtaining the initial bounded velocity distribution are different.

Consider the evolution of a fiber with the initial bounded velocity distribution

$$\dot{\xi}(z,0) = V_0 e^{-\frac{z^2}{a^2}}. \tag{A1}$$

Introducing the dimensionless variables (marked by primes), $z = az'$, $t = \frac{a^2}{\beta_c}t'$, $\xi = V_0\frac{a^2}{\beta_c}\xi'$, the equations of a fiber vibration together with initial conditions are written in the form

$$\frac{\partial^2\xi'}{\partial t'^2} = -\frac{\partial^4\xi'}{\partial z'^4}, \tag{A2}$$

$$\frac{\partial\xi'(z,0)}{\partial t'} = e^{-z'^2}. \tag{A3}$$

Primes hereafter will be omitted. One needs to find the solution for the velocities of the fiber points at an arbitrary time. Applying the Fourier transform, we obtain

$$\begin{aligned}\dot{\xi}(z,t) &= \pi^{1/2}\int\frac{dk}{2\pi}\cos\left(k^2t\right)\exp\left(-\frac{k^2}{4}+ikz\right)\\ &= \frac{1}{2}\pi^{1/2}\int\frac{dk}{2\pi}\left[\exp\left(-\frac{k^2}{4}+ikz+ik^2t\right)\right.\\ &\quad\left.+\exp\left(-\frac{k^2}{4}+ikz-ik^2t\right)\right].\end{aligned} \tag{A4}$$

Evaluating the Gaussian integrals gives the result

$$\begin{aligned}\dot{\xi}(z,t) &= \frac{1}{4}\left[\frac{1}{\left(\frac{1}{4}+it\right)^{1/2}}\exp\left(-\frac{z^2}{1+4it}\right)+\frac{1}{\left(\frac{1}{4}-it\right)^{1/2}}\right.\\ &\quad\left.\times\exp\left(-\frac{z^2}{1-4it}\right)\right] = \frac{1}{2}\exp\left(-\frac{z^2}{1+16t^2}\right)\\ &\quad\times\left[a_1(t)\cos\left(\frac{4tz^2}{1+16t^2}\right)+ia_2(t)\sin\left(\frac{4tz^2}{1+16t^2}\right)\right],\end{aligned} \tag{A5}$$

where

$$a_1(t) = \frac{1}{(1+4it)^{1/2}}+\frac{1}{(1-4it)^{1/2}},$$
$$a_2(t) = \frac{1}{(1+4it)^{1/2}}-\frac{1}{(1-4it)^{1/2}}$$

Extracting the roots, we have

$$(1\pm4it)^{1/2} = (1+16t^2)^{1/4}\exp\left(\pm i\frac{1}{2}\arctan4t\right),$$

$$\cos\left(\frac{1}{2}\arctan4t\right) = \left\{\frac{1}{2}\left[(1+16t^2)^{1/2}+1\right]\right\}^{1/2}\frac{1}{(1+16t^2)^{1/4}},$$

$$\sin\left(\frac{1}{2}\arctan4t\right) = \left\{\frac{1}{2}\left[(1+16t^2)^{1/2}-1\right]\right\}^{1/2}\frac{1}{(1+16t^2)^{1/4}}.$$

Using these expressions, we define

$$\dot{\xi}(z,t) = \frac{\exp\left(-\frac{z^2}{1+16t^2}\right)}{2^{1/2}(1+16t^2)^{1/2}}\left\{\left[(1+16t^2)^{1/2}+1\right]^{1/2}\cos\left(\frac{4tz^2}{1+16t^2}\right)+\left[(1+16t^2)^{1/2}-1\right]^{1/2}\sin\left(\frac{4tz^2}{1+16t^2}\right)\right\}. \tag{A6}$$

For the displacements of the fiber points we obtain the following expression in dimensional form:

$$\xi(z,t) = V_0\frac{1}{2^{1/2}}\int_0^t\frac{dt'}{\left(1+16\beta_c^2t'^2/a^4\right)^{1/2}}f(z,t')\exp\left(-\frac{z^2/a^2}{1+16\beta_c^2t'^2/a^4}\right), \tag{A7}$$

where

$$f(z,t') = [g(t')+1]^{1/2}\cos\left(\frac{4\beta_ct'z^2/a^4}{1+16\beta_c^2t'^2/a^4}\right)+[g(t')-1]^{1/2}\sin\left(\frac{4\beta_ct'z^2/a^4}{1+16\beta_c^2t'^2/a^4}\right),$$

$$g(t') = \left(1+16\beta_c^2t'^2/a^4\right)^{1/2}.$$

The displacement of the central point is

$$\xi(0,t) = V_0 \frac{1}{2^{1/2}} \int_0^t dt' \frac{\left[\left(1+16\beta_c^2 t'^2/a^4\right)^{1/2}+1\right]^{1/2}}{\left(1+16\beta_c^2 t'^2/a^4\right)^{1/2}}. \tag{A8}$$

For long time intervals, $t \gg a^2/\beta_c$, the displacement of the central point increases with time as

$$\xi(0,t) = V_0 \frac{a}{8^{1/2}\beta_c^{1/2}} t^{1/2} + \text{const}. \tag{A9}$$

Similar computations may be performed for deformation of the infinite plate. The equation for the bending of the plate with thickness h situated in the xy plane is

$$\rho h \frac{\partial^2 \xi}{\partial t^2} = -D\Delta^2 \xi,\ D = \frac{Eh^3}{12(1-\sigma^2)},\ \Delta = \frac{\partial^2}{\partial x^2} + \frac{\partial^2}{\partial y^2}. \tag{A10}$$

The dispersion equation for the plate vibrations is

$$\omega^2(k) = \beta^2 k^4,\ k^2 = k_x^2 + k_y^2,\ \ \beta^2 = \frac{D}{\rho h}.$$

Assume that the initial velocity distribution is given by $V(r) = V_0 e^{-(r/a)^2}$. Similar to the problem with fibers, we perform the Fourier transform with respect to the x and y coordinates and find the distribution of the velocity and displacement along the plate:

$$\dot{\xi}(r,t) = V_0 f(r,t),\ \ \xi(r,t) = V_0 \int_0^t dt' f(r,t'), \tag{A11}$$

where

$$f(r,t) = \frac{a^4}{a^4+16\beta^2 t^2} \exp\left(-\frac{r^2 a^2}{a^4+16\beta^2 t^2}\right) \times \left[\cos\left(\frac{4\beta t r^2}{a^4+16\beta^2 t^2}\right) + \frac{4\beta t}{a^2} \sin\left(\frac{4\beta t r^2}{a^4+16\beta^2 t^2}\right)\right].$$

In the vicinity of the origin, the displacement is

$$\xi(r,t) \approx V_0 \frac{a^2}{4\beta}\left[\arctan\left(\frac{4\beta t}{a^2}\right) - \frac{r^2 4\beta t}{a^4+16\beta^2 t^2}\right]. \tag{A12}$$

At long times the displacement is constant,

$$\xi(r,t) = V_0 \frac{\pi a^2}{8\beta}. \tag{A13}$$

Comparing Eq. (A9) with Eq. (A13), we see that at long times the deformation of the infinite plate at the region of collision attains a constant value, while for an infinitely long fiber it tends to infinity. This difference is explained by the following: the energy of deformation of a plate is greater than that of a fiber at the same displacements ξ and length scales d. Following [16], the energy of elastic deformation of the plate is of the order $W_p \approx \frac{Eh^3}{24(1-\sigma^2)}\frac{\xi^2}{d^2}$, while that of the fiber is $W_f \approx \frac{E\pi r_0^4}{8}\frac{\xi^2}{d^3}$. At sufficiently large values of d the energy of deformation of the plate is greater than that of the fiber, $W_p \gg W_f$.

We now consider the torsional vibrations. The dynamics of the angle $\varphi(z,t)$ of the torsional vibrations is described by the standard wave equation,

$$\rho I_1 \frac{\partial^2 \varphi}{\partial t^2} = C \frac{\partial^2 \varphi}{\partial z^2}, \tag{A14}$$

in which the velocity of propagation of a perturbation is $u = (C/\rho I_1)^{1/2}$. Assuming a linear law of dispersion, it is not difficult to account for the finite length of the fiber. The general solution for the wave equation with zero initial condition is

$$\varphi(z,t) = f(z+ut) - f(z-ut). \tag{A15}$$

The function $f(z)$ is dependent on the initial angular velocity $\omega(z,0) = \omega_n(z)$:

$$\frac{\partial \varphi(z,0)}{\partial t} = 2u\frac{df(z)}{dz} = \omega_n(z).$$

The angular velocity is governed by the same equation as the angle. At an arbitrary time and with initial conditions $\omega(0,t) = \omega(L,t) = 0$, the angular velocity is equal to

$$\omega(z,t) = \frac{1}{2}\sum_n [\omega_n(z-2nL-ut) - \omega_n(2L-z-2nL-ut) + \omega_n(z-2nL+ut) - \omega_n(2L-z-2nL+ut)], \tag{A16}$$

where the function $\omega_n(z)$ is assumed to be equal to zero outside the interval $0 < z < L$. The function $\omega(z,t)$ is periodic, with a period of $2t_0 = 2L/u$, and possesses the following property: $\omega(z,t+t_0) = -\omega(L-z,t)$. If the initial distribution of the angular velocity is symmetric with respect to the middle of the fiber, $\omega_n(z) = \omega_n(L-z)$, then the angular velocity in a t_0 period will be reproduced with a different sign:

$$\omega(z,t+t_0) = -\omega(z,t). \tag{A17}$$

APPENDIX B: MULTIPLE COLLISIONS OF LARGE PARTICLES WITH A FINE FIBER

During the time between contact interactions, which for a fine fiber is $\sim 1/\omega_1$, the highest harmonics make several oscillations and obtain a random phase. Therefore, the excitation of the highest harmonics in the process of the contact interaction may be neglected. With this in mind, for an approximate description of the multiple collisions, in the expansion over modes $\boldsymbol{\xi}(z,t)$ we leave only the first harmonic of the fiber vibrations, $\boldsymbol{\xi}(z,t) = \boldsymbol{\xi}_1(t)\sin(\pi z/L)$. Thus, the following system of equations is obtained from Eqs. (2) and (8) for $z_0 = L/2$, which is similar to that used to describe the two-particle dynamics:

$$m_0 \frac{d^2\boldsymbol{\xi}_1}{dt^2} = -k\boldsymbol{\xi}_1 + \mathbf{F},\ m_0 = \frac{1}{2}\rho S l,\ k = \frac{\pi^4 EI}{2L^3}, \tag{B1}$$

$$m\frac{d^2\mathbf{r}}{dt^2} = -\mathbf{F}, \tag{B2}$$

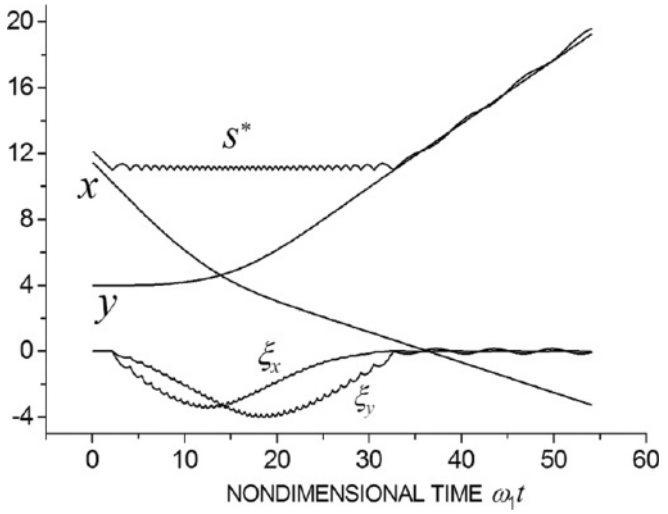

FIG. 11. Dimensionless coordinates of the particle (x, y), the fiber (ξ_x, ξ_y), and the relative distance s^* versus time in the process of multiple collisions. All coordinates are brought to nondimensional form by division with the radius of the fiber r_0.

where $\mathbf{F}$ is the van der Waals force [see Eq. (C3)]. For elastic contact interactions we find the following condition relating initial and final velocities:

$$\dot{\boldsymbol{\xi}}_1' = \dot{\boldsymbol{\xi}}_1 - 2[(\dot{\boldsymbol{\xi}}_1 - \mathbf{u}) \cdot \mathbf{n}]\mathbf{n},$$

$$\dot{\mathbf{r}}' = \dot{\mathbf{r}} - 2[(\dot{\mathbf{r}} - \mathbf{u}) \cdot \mathbf{n}]\mathbf{n},$$

where $\mathbf{n}$ is the normal vector given by Eq. (12) and $\mathbf{u}$ represents the velocity of the center of mass prior to collision,

$$\mathbf{u} = \frac{m_0 \dot{\boldsymbol{\xi}}_1 + m\dot{\mathbf{r}}}{m_0 + m}.$$

Figure 11 illustrates the time dynamics of multiple collisions of a particle with radius $R = 1\ \mu$m and mass $m = 4.19 \times 10^{-11}$ g, moving with velocity $V_0 = 200$ cm/s, with the fine fiber radius $r_0 = 0.1\ \mu$m, length $L = 100\, r_0$, mass $m_0 = 3.14 \times 10^{-13}$ g, and dimensionless eigenfrequency $\omega_1 R/V_0 = (k/m_0)^{1/2} R/V_0 = 17.4$. All linear dimensions were scaled with r_0. As seen from the results of the calculations, at $\omega_1 R/V_0 \gg 1$, after the collision, the fiber moves a small distance from the particle, $s^* - R - r_0 \equiv |\boldsymbol{\xi} - \mathbf{r}| - R - r_0 \ll R$, where s^* stands for the distance between the particle center and the fiber axis. In this case the collision model can be further simplified if we consider that the fiber is sliding at the particle surface until complete detachment (see Fig. 12). If the van der Waals forces are neglected, then the collision process in this approximation is described by the action $S = \int \Lambda dt$ with the Lagrange function [28]

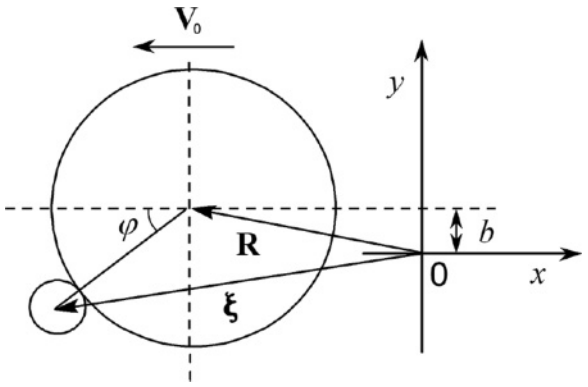

FIG. 12. Sketch of the collision of a large particle having velocity V_0 with a fine fiber, where $\boldsymbol{\xi}$ is the fiber displacement from the equilibrium position at the point of contact with a particle, $\mathbf{R}$ is the particle position, and b is the shooting distance. The origin of the coordinates is chosen to be at the axis of the nondeformed fiber.

$$\Lambda = \frac{m}{2}(\dot{x}^2 + \dot{y}^2) + \frac{m_0}{2}(\dot{x}\cos\varphi + \dot{y}\sin\varphi)^2 + \frac{m_0}{2}(R + r_0)^2\dot{\varphi}^2 - \frac{k}{2}\{[x - (R + r_0)\cos\varphi]^2 + [y - (R + r_0)\sin\varphi]^2\}. \tag{B3}$$

Equalizing the variational derivative of the action to zero with respect to x, y, and φ, we obtain the equations of motion, while varying with respect to R yields the condition for detachment. In this Appendix we will not spell out a complete system of equations, focusing our attention only on the interaction of a fiber with a massive particle moving with constant velocity $\dot{x} = -V_0$. Varying Eq. (B3) with respect to φ, we obtain

$$m_0(R + r_0)^2\ddot{\varphi} = -\frac{m_0}{2}\dot{x}^2 \sin 2\varphi - k(R + r_0)(x\sin\varphi - y\cos\varphi). \tag{B4}$$

Varying the Lagrange function with respect to R, the condition for particle detachment from the fiber surface is obtained:

$$m_0(R + r_0)\dot{\varphi}^2 + k[x\cos\varphi + y\sin\varphi - (R + r_0)] > 0. \tag{B5}$$

The detachment condition is written in the following form by accounting for the van der Waals forces:

$$m_0(R + r_0)\dot{\varphi}^2 + k[x\cos\varphi + y\sin\varphi - (R + r_0)] > \frac{AR}{6\varepsilon^2}. \tag{B6}$$

It is seen from Eq. (B4) that at sufficiently long times the force acting on the fiber is governed by the term that is dependent on the x coordinate. When the angle φ is increased, the conditions given by Eq. (B5) or by Eq. (B6) are violated, and thus, the particle is detached from the fiber. The given analysis shows that, in the process of multiple collisions, a fast, large particle may deflect a fiber to its radius and move farther. In this case, the time of interaction is of the order of the flight time, R/V_0. The required energy of deformation is given by

$$W = \frac{1}{2}EI\int\left(\frac{\partial^2\boldsymbol{\xi}}{\partial z^2}\right)^2 dz = EI\boldsymbol{\xi}_0^2\frac{\pi^4}{4L^3}.$$

A particle moves with a slight deflection from a straight trajectory if

$$\frac{mV_0^2}{2} \gg W.$$

By letting $\xi_0^2 = R^2$, the kinetic energy required for fiber deformation is found from

$$\frac{mV_0^2}{2} \gg EIR^2\frac{\pi^4}{4L^3}.$$

This condition is compatible with that for the long-term contact of a particle with a fiber, $\omega_1 R/V_0 \gg 1$, for sufficiently large and heavy particles with $m/m_0 \gg 4(\omega_1 R/V_0)^2$.

APPENDIX C: VAN DER WAALS' FORCES BETWEEN A SPHERICAL PARTICLE AND A CYLINDER

For estimating the van der Waals interaction between two bodies, let us use the method of summation of energies of the interaction of single atoms in two bodies for the cases of nonretarded $U \sim 1/r^6$ and retarded interaction $U \sim 1/r^7$, where r is the interatomic distance. Here we consider only the interaction of a ball and a half-space, which is valid if the gap between a ball and a cylinder is smaller than the cylinder radius. For an arbitrary point inside a ball located at a distance H from the boundary surface, introducing a cylindrical system of coordinates with its origin in this point and with the z axis oriented normally to the boundary surface, we obtain

$$U_w(H) \sim \int_H^\infty dz_2 d\varphi_2 \int_0^\infty \rho_2 d\rho_2 \frac{1}{\left(z_2^2+\rho_2^2\right)^{n/2}} = \frac{2\pi}{n-2}\int_H^\infty dz_2 d\varphi_2 \frac{1}{z_2^{n-2}} = \frac{2\pi}{(n-2)(n-3)H^{n-3}}.$$

Expressing H for the chosen point in the spherical system of coordinates in terms of the distance h between the center of the ball and the surface as $H = h - \rho_1\cos\theta_1$, we obtain

$$U_w \sim \frac{2\pi}{(n-2)(n-3)}\int_0^R \rho_1^2 d\rho_1 \sin\theta_1 d\theta_1 d\varphi_1 \times \frac{1}{(h-\rho_1\cos\theta_1)^{n-3}} = \frac{4\pi^2}{(n-2)(n-3)(n-4)} \times \int_0^R \rho_1 d\rho_1 \left[\frac{1}{(h-\rho_1)^{n-4}} - \frac{1}{(h+\rho_1)^{n-4}}\right].$$

For the interaction force we derive the following expressions:

$$F_w = -\frac{dU_w}{dh} = \frac{4\pi^2}{(n-2)(n-3)} \times \int_0^R \rho_1 d\rho_1 \left[\frac{1}{(h-\rho_1)^{n-3}} - \frac{1}{(h+\rho_1)^{n-3}}\right]$$

$$= \frac{4\pi^2}{(n-2)(n-3)(n-4)}\left\{\frac{R}{(h-R)^{n-4}} + \frac{R}{(h+R)^{n-4}} - \frac{1}{(n-5)}\left[\frac{1}{(h-R)^{n-5}} - \frac{1}{(h+R)^{n-5}}\right]\right\}, \quad \text{(C1)}$$

where $n = 6$ and $n = 7$ for the nonretarded and retarded interactions, respectively. Expressing the coefficient of proportionality in terms of the Hamaker constant A and noting that $h = r - r_0$, we derive the nonretarded force

$$F_6 = -\frac{2A}{3r_0}\frac{(R/r_0)^3}{\left[(r-1)^2-(R/r_0)^2\right]^2}.$$

Hereinafter r denotes the dimensionless ratio r/r_0. Using the notation $A_{\rm ret}$ for the constant of the retarded van der Waals interaction between macroscopic bodies, the force of the van der Waals interaction with retardation is expressed as

$$F_7 = -\frac{8A_{\rm ret}}{15r_0^2}\frac{(R/r_0)^3(r-1)}{[(r-1)^2-(R/r_0)^2]^3}.$$

For an arbitrary fiber radius the force of the nonretarded interaction was derived in [29]:

$$F_6 = -\frac{A}{24r_0}\frac{(R/r_0)^3}{p^{3/2}s^2r^{5/2}}[(3+t^2)E(p^{-1}) - stK(p^{-1})], \quad \text{(C2)}$$

where $p = 1 + s/2, t = 1 + s, s = [(r-1)^2 - (R/r_0)^2]/(2r)$, E and K are complete elliptic integrals, $r = 1 + x + R/r_0$, and x is the dimensionless gap between the particle and the cylinder. For small gaps, $x \ll \min(R/r_0, 1)$, and Eq. (C2) reduces to

$$F_6 = -\frac{AR}{6x^2r_0^2}\left(\frac{r_0}{R+r_0}\right)^{1/2},$$

which coincides with Eq. (3) used in the text for $x \gg \varepsilon/r_0$. The force of the retarded ball-cylinder interaction is expressed in terms of the cumbersome one-dimensional integral [30], which is not given here.

In a wide range of distances the force can be approximated by the following piecewise function:

$$F(r) = \left\{1 + \frac{R+\varepsilon}{r_0} \leqslant r \leqslant r_{67}, F_6; r > r_{67}, F_7\right\}. \quad \text{(C3)}$$

Here the radius r_{67} roughly distinguishes the distance range into unretarded and fully retarded regions and is estimated from the following condition: $F_6 = F_7$. To exclude the contact singularity, the obtained force is cutoff at the gap $\varepsilon = 4$ Å, where the forces of repulsion begin to act.

[1] A. A. Kirsch, and I. B. Stechkina, in *Fundamentals of Aerosol Science*, edited by D. T. Shaw (Wiley, New York, 1978), pp. 165–256.

[2] K. C. Fan, B. Wamsley, and J. W. Gentry, J. Colloid Interface Sci. **65**, 162 (1978).

[3] P. F. Dunn and K. J. Renken, Aerosol Sci. Technol. **7**, 97 (1987).

[4] H. J. Rembor, R. Maus, and H. Umhauer, Part. Part. Syst. Charact. **16**, 54 (1999).

[5] M. J. Ellenbecker, D. Leith, and J. M. Price, J. Air Pollut. Control Assoc. **30**, 1224 (1980).

[6] B. Dahneke, J. Colloid Interface Sci. **37**, 342 (1971).
[7] N. A. Fuchs, *Mechanics of Aerosols* (Pergamon, Oxford, 1964).
[8] R. A. Wessel and J. Righi, Aerosol Sci. Technol. **9**, 29 (1988).
[9] S. P. Timoshenko, *Strength and Vibrations of Constructions: Selected Works* (Nauka, Moscow, 1975), in Russian.
[10] N. A. Kilchevski, *Dynamic Contact Compression of Rigid Bodies: Impact* (Naukova Dumka, Kiev, 1976), in Russian.
[11] C. V. Raman, Phys. Rev. **15**, 277 (1920).
[12] C. Zener, Phys. Rev. **59**, 669 (1941).
[13] Aerosol Sci. Technol. **23**(1), (1995).
[14] O. V. Kim and P. F. Dunn, J. Aerosol Sci. **38**, 532 (2007).
[15] C. Thornton, Powder Technol. **192**, 152 (2009).
[16] L. D. Landau and E. M. Lifshitz, *Theory of Elasticity*, 3rd ed. (Butterworth-Heinemann, Oxford, 1986), Vol. 7.
[17] B. V. Derjaguin, N. V. Churaev, and V. M. Muller, *Surface Forces* (Consultants Bureau, New York, 1987).
[18] K. L. Johnson, *Contact Mechanics*, 2nd ed. (Cambridge University Press, New York, 1987).
[19] K. L. Johnson, K. Kendall, and A. W. Roberts, Proc. R. Soc. London, Ser. A **324**, 301 (1971).
[20] D. Tabor, J. Colloid Interface Sci. **58**, 2 (1977).
[21] V. M. Muller, V. S. Yushchenko, and B. V. Derjaguin, J. Colloid Interface Sci. **77**, 91 (1980).
[22] W. Cheng, P. F. Dunn, and R. M. Brach, J. Adhesion **78**, 929 (2002).
[23] G. Kasper, S. Schollmeier, J. Meyer, and J. Hoferer, J. Aerosol Sci. **40**, 993 (2009).
[24] S. Kuwabara, J. Phys. Soc. Jpn. **14**, 527 (1959).
[25] E. Hairer, S. Norsett, and G. Wanner, *Solving Ordinary Differential Equations I: Nonstiff Problems*, 2nd ed. (Springer-Verlag, Berlin, 1993).
[26] L. A. Santalo, *Integral Geometry and Geometric Probability* (Addison-Wesley, London, 1976).
[27] H. J. Rembor and G. Kasper, in *PARTEC 98, 4th European Symposium on Separation of Particles from Gases* (*NurnbergMesse GmbH, MesseCentrum, Germany*, 1998), p. 223.
[28] L. D. Landau and E. M. Lifshitz, *Mechanics*, 3rd ed. (Butterworth-Heinemann, Oxford, 1976), Vol. 1.
[29] J. I. Rosenfeld and D. T. Wasan, J. Colloid Interface Sci. **47**, 27 (1974).
[30] V. A. Kirsch, Adv. Colloid Interface Sci. **104**, 311 (2003).